JCTC Journal of Chemical Theory and Computation

Franck−Condon Simulations including Anharmonicity of the $\tilde{A}^1A''-\tilde{X}^1A'$ Absorption and Single Vibronic Level Emission Spectra of HSiCl and DSiCl

Daniel W. K. Mok,*,† Edmond P. F. Lee,*,†,‡ Foo-tim Chau,† and John M. Dyke‡

Department of Applied Biology and Chemical Technology, the Hong Kong Polytechnic University, Hung Hom, Hong Kong, and School of Chemistry, University of Southampton, Highfield, Southampton SO17 1BJ, U.K.

Received November 28, 2008

Abstract: RCCSD(T) and/or CASSCF/MRCI calculations have been carried out on the $\tilde{X}^1A'$ and $\tilde{A}^1A''$ states of HSiCl employing basis sets of up to the aug-cc-pV5Z quality. Contributions from core correlation and extrapolation to the complete basis set limit were included in determining the computed equilibrium geometrical parameters and relative electronic energy of these two states of HSiCl. Franck−Condon factors which include allowance for anharmonicity and Duschinsky rotation between these two states of HSiCl and DSiCl were calculated employing RCCSD(T) and CASSCF/MRCI potential energy functions, and were used to simulate the $\tilde{A}^1A'' \leftarrow \tilde{X}^1A'$ absorption and $\tilde{A}^1A'' \rightarrow \tilde{X}^1A'$ single vibronic level (SVL) emission spectra of HSiCl and DSiCl. Simulated absorption and experimental LIF spectra, and simulated and observed $\tilde{A}^1A''(0,0,0) \rightarrow \tilde{X}^1A'$ SVL emission spectra, of HSiCl and DSiCl are in very good agreement. However, agreement between simulated and observed $\tilde{A}^1A''(0,1,0) \rightarrow \tilde{X}^1A'$ and $\tilde{A}^1A''(0,2,1) \rightarrow \tilde{X}^1A'$ SVL emission spectra of DSiCl is not as good. Preliminary calculations on low-lying excited states of HSiCl suggest that vibronic interaction between low-lying vibrational levels of the $\tilde{A}^1A''$ state and highly excited vibrational levels of the $\tilde{a}^3A''$ is possible. Such vibronic interaction may change the character of the low-lying vibrational levels of the $\tilde{A}^1A''$ state, which would lead to perturbation in the SVL emission spectra from these vibrational levels.

Introduction

In their continuing study of the spectroscopy of carbenes, silylenes, and germylenes, reactive intermediates important for chemical vapor deposition (CVD) processes in the semiconductor industry, the Clouthier group recorded laser induced fluorescence (LIF) spectra of HSiCl and DSiCl produced in an electric discharge of $SiHCl_3$ and $SiDCl_3$, respectively, diluted in Ar through a pulsed jet.[1] This work was performed over a decade ago. A few years later, they published single vibronic level (SVL) emission spectra of HSiCl and DSiCl.[2] In this SVL emission (or dispersed fluorescence) study, they employed data from harmonic force field and density functional theory (DFT) calculations using the B3LYP functional and the 6−311G(3df,3pd) basis set to simulate the $\tilde{A}^1A''(0,0,0) \rightarrow \tilde{X}^1A'$ SVL emission spectrum of HSiCl, using computed Franck−Condon (FC) factors obtained within the harmonic oscillator model. Agreements between simulated and observed SVL emission spectra are reasonably good, particularly for the main $\tilde{A}^1A''(0,0,0) \rightarrow \tilde{X}^1A'(0,v_2'',0)$ vibrational progression. However, for the weak vibrational structure, there are clearly noticeable discrepancies between simulated and observed SVL spectra. Specifically, in addition to the main $\tilde{A}^1A''(0,0,0) \rightarrow \tilde{X}^1A'(0,v_2'',0)$ progression, simulated spectra show only one relatively weak $\tilde{A}^1A''(0,0,0) \rightarrow \tilde{X}^1A'(1,v_2'',0)$ progression, but in the experimental SVL spectrum the only observed weak progression is the $\tilde{A}^1A''(0,0,0) \rightarrow \tilde{X}^1A'(0,v_2'',1)$ progression (vide infra). The $\tilde{A}^1A''(0,0,0) \rightarrow \tilde{X}^1A'(1,v_2'',0)$ progression was not observed in the experimental SVL emission spectrum as

* To whom correspondence should be addressed. E-mail: Daniel@polyu.edu.hk (D.W.K.M.); epl@soton.ac.uk (E.P.F.L.).

† The Hong Kong Polytechnic University.

‡ University of Southampton.

10.1021/ct800513v CCC: $40.75
Published on Web 02/12/2009

predicted by harmonic FC simulation. It was concluded that, "Obtaining reliable simulations of these spectra will be a stringent test of future Franck−Condon calculations which include vibrational anharmonicity."[2] In this connection, we propose, in the present investigation, to carry out state-of-the-art *ab initio* calculations on the $\tilde{X}^1A'$ and $\tilde{A}^1A''$ states of HSiCl and FC factor calculations between these two states, which include allowance for anharmonicity and Duschinsky rotation, aiming to obtain better agreement between theory and experiment.

For earlier spectroscopic and computational studies on HSiCl, Clouthier et al. has given thorough discussions previously,[1,2] and hence they will not be repeated here. After the above-mentioned LIF and SVL emission studies on HSiCl/DSiCl were published,[1,2] microwave spectra of $H^{28}Si^{35}Cl$, $H^{28}Si^{37}Cl$, $H^{29}Si^{35}Cl$, and $H^{30}Si^{35}Cl$ were measured at 14−15 GHz, and the effective rotational constants, chlorine nuclear quadrupole coupling constants, and nuclear spin-rotation constants of the four isotopomers were determined.[3] The molecular structure of HSiCl derived from this study is essentially identical to those reported in references 1 and 2. In addition, the ^{35}Cl nuclear quadrupole coupling constant in HSiCl was calculated at up to the MP3 level. A LIF and dispersed fluorescence study of HSiCl, produced in the UV photodissociation of 2-chloroethenylsilane, has also been published, and it was concluded that emission spectra of HSiCl could be useful to monitor the CVD process of 2-chloroethenylsilane.[4] On the computational front, a number of high-level *ab initio* studies have been carried out recently on the $\tilde{X}^1A'$ state of HSiCl.[5−7] The latest study reported CCSD(T) calculations of nuclear-spin-rotation and nuclear quadrupole coupling constants of some halocarbenes and halosilylenes, including HSiCl.[7] However, for the $\tilde{A}^1A''$ state of HSiCl, to our knowledge, the only available calculations are the above-mentioned B3LYP/6−311G(3df,3pd) calculations reported in ref 2.

Related closely to the present study, we have recently reported a combined *ab initio*/FC study on the SVL emission spectra of HSiF and DSiF.[8] In this work, very good agreement between simulated and observed spectra was obtained for the $\tilde{A}^1A''(1,0,0) \rightarrow \tilde{X}^1A'$ SVL emission of HSiF and the $\tilde{A}(0,0,0) \rightarrow \tilde{X}^1A'$ and $\tilde{A}(0,1,0) \rightarrow \tilde{X}^1A'$ SVL emissions of DSiF. However, discrepancies between simulated and observed spectra of the $\tilde{A}(0,1,0) \rightarrow \tilde{X}^1A'$ and $(1,1,0) \rightarrow \tilde{X}^1A'$ SVL emissions of HSiF have been found. It was concluded that they were most likely, partly, caused by experimental deficiencies and, partly, by inadequacies in the *ab initio* levels of theory employed in the calculation of the potential energy functions (PEFs). Nevertheless, on the basis of computed FC factors, minor revisions of previous vibrational assignments have been suggested (see ref 8 for details).

Computational Details

Ab Initio Calculations. RCCSD(T)[9,10] and CASSCF/MRCI[11,12] geometry optimization calculations were carried out on the $\tilde{X}^1A'$ state of HSiCl, while only CASSCF/MRCI calculations were performed on the lowest open-shell singlet $\tilde{A}^1A''$ state. For the closed-shell $\tilde{X}^1A'$ state, the computed T_1 diagnostics (<0.013 in all cases) obtained from RCCSD(T) calculations and the calculated CI coefficients (>0.92 for the main ground-state electronic configuration) from the computed CASSCF and MRCI wave functions indicate that multireference character is negligibly small for this state at the computed equilibrium geometries. Therefore, it can be concluded that the size-consistent, single-reference RCCSD(T) method should be the more suitable, and more reliable than the size-inconsistent MRCI method, for the $\tilde{X}^1A'$ state of HSiCl. Nevertheless, CASSCF/MRCI calculations were also carried out for the $\tilde{X}^1A'$ state to obtain relative electronic energies between the $\tilde{X}^1A'$ state and the $\tilde{A}^1A''$ state because the latter is an open-shell singlet state, which cannot be adequately treated by a single electronic configuration and hence requires a multireference method. It should be noted that all CASSCF/MRCI calculations carried out in the present study are single state (i.e., not average-state) calculations, with the CASSCF wave function (i.e., the CASSCF molecular orbitals and reference configurations to be used in subsequent MRCI calculations) optimized for the single state concerned (i.e., the $\tilde{X}^1A'$ state or the $\tilde{A}^1A''$ state). The CASSCF/MRCI wave functions thus obtained are optimal for the state concerned.

Correlation-consistent basis sets of aug-cc-pVQZ (AVQZ), aug-cc-pV5Z (AV5Z), and aug-cc-pwCVQZ (ACVQZ) qualities have been used in the present investigation. For H, the standard aug-cc-pVQZ and aug-cc-pV5Z basis sets[13] were used. With the AVQZ and AV5Z quality basis sets, the aug-cc-pV(Q+d)Z and aug-cc-pV(5+d)Z basis sets[14] were used for the second row elements, Si and Cl, and a full valence active space was employed in the CASSCF and MRCI calculations, while the default frozen core was employed in the RCCSD(T) calculations. Results obtained from calculations employing the AVQZ and AV5Z basis sets were used to estimate contributions on extrapolation to the complete basis set (CBS) limit to the optimized geometrical parameters and computed relative electronic energies. Two extrapolation techniques were used. First, the correction took half of the difference between the computed CCSD(T) or CASSCF/MRCI+D (D denoting the inclusion of Davidson corrections[15]) values (i.e., optimized geometrical parameters or computed relative electronic energies) obtained using the AVQZ and AV5Z basis sets.[16] Second, the extrapolation technique, which employed the $1/X^3$ formula[17] with the computed values (i.e., optimized geometrical parameters or computed relative electronic energies) obtained using the AVQZ and AV5Z basis sets, was used. With the ACVQZ quality basis sets, the aug-cc-pwCVQZ basis sets[18] were used for Si and Cl, and the RCCSD(T) and CASSCF/MRCI calculations that were carried out employed both the default frozen core, and also the core with only the Si $1s^2$ and Cl $1s^2$ electrons frozen. Results obtained from these calculations with the ACVQZ basis sets were used to estimate contributions from including the $2s^22p^6$ core electrons of Si and Cl in the correlation treatments to the optimized geometrical parameters and computed relative electronic energies. The estimated contributions of basis size extrapolation to the CBS limit and core electron correlation to the optimized geo-

metrical parameters and computed relative electronic energies have been assumed to be additive.

All *ab initio* calculations carried out in the present study, including the energy scans for the potential energy surfaces to be described below, have employed the MOLPRO suite of programs.[19]

Potential Energy Functions, Variational Calculations of Anharmonic Vibrational Wave Functions, and Franck−Condon Factor Calculations. RCCSD(T) and CASSCF/MRCI+D potential energy functions (PEFs) for the $\tilde{X}^1A'$ and $\tilde{A}^1A''$ states of HSiCl, respectively, were obtained by fitting the following polynomial to calculated *ab initio* total electronic energies {RCCSD(T)/AV5Z and CASSCF/MRCI+D/AV5Z energies, respectively}:

$$\mathbf{V} = \sum_{ijk} C_{ijk}(S_1)^i(S_2)^j(S_3)^k + V_{\mathrm{eqm}} \quad (1)$$

In the above expression of the PEF, S_2 is the bending coordinate of Carter and Handy,[20] $S_2 = \Delta\theta + \alpha\Delta\theta^2 + \beta\Delta\theta^3$, where $\Delta\theta$ is the displacement of the bond angle from the equilibrium value, $(\theta - \theta_e)$. S_1 and S_3 are the displacements of the HSi and SiCl bond lengths from the equilibrium values, $(r - r_e)$, respectively; 377 CCSD(T)/AV5Z energy points in the ranges of $1.25 \le r(\mathrm{HSi}) \le 1.99$ Å, $70.0 \le \theta(\mathrm{HSiCl}) \le 130.0°$, and $1.81 \le r(\mathrm{SiCl}) \le 2.55$ Å scanned for the $\tilde{X}^1A'$ state and 559 CASSCF/MRCI+D/AV5Z energy points in the ranges of $1.29 \le r(\mathrm{HSi}) \le 2.45$ Å, $75.0 \le \theta(\mathrm{HSiCl}) \le 163.0°$, and $1.83 \le r(\mathrm{SiCl}) \le 2.60$ Å scanned for the $\tilde{A}^1A''$ state were used in the fitting of the PEFs. The nonlinear least-squares fit procedure, NL2SOL,[21] was employed to obtain the C_{ijk} values (with the restriction of $i + j + k \ge 2$; vide infra), V_{eqm}, r_e, θ_e, α, and β from the computed single point energy data.

For both the $\tilde{X}^1A'$ and the $\tilde{A}^1A''$ states, variational calculations, which employed the rovibronic Hamiltonian of Watson[22] for a nonlinear molecule, were carried out to obtain the anharmonic vibrational wave functions and energies. The anharmonic vibrational wave functions were expressed as linear combinations of harmonic oscillator functions, $h(v_1, v_2, v_3)$, where v_1, v_2, and v_3 denote the quantum numbers of the harmonic basis functions for the HSi stretching, HSiCl bending, and SiCl stretching modes, respectively, as described previously.[23] Harmonic basis functions with vibrational quantum numbers up to $h(7, 16, 16)$ and a restriction of $v_1 + v_2 + v_3 \le 16$ were included in the variational calculations of the $\tilde{X}^1A'$ state of both HSiCl and DSiCl. For the $\tilde{A}^1A''$ state, harmonic basis functions up to $h(9, 12, 12)$, with a restriction of $v_1 + v_2 + v_3 \le 12$ were considered for HSiCl. For the $\tilde{A}^1A''$ state of DSiCl, harmonic basis functions up to $h(8, 12, 12)$ were included. FC factors were calculated employing computed anharmonic vibrational wave functions and with allowance for Duschinsky rotation, as described previously.[24] The best estimated computed geometrical parameters of the two states (vide infra) were used in the FC calculations. Employing these computed FC factors for spectral simulations gave the best theoretical simulated spectra.

In spectral simulations, vibrational components of the $\tilde{A}^1A'' \rightarrow \tilde{X}^1A'$ SVL emission spectra of HSiCl and DSiCl were simulated using Gaussian functions with a full-width-at-half-maximum (fwhm) of 10 cm^{-1}. The relative intensity of each vibrational component in a simulated SVL emission spectrum was expressed as the product of the corresponding computed anharmonic FC factor and a frequency factor of power four. For simulations of $\tilde{A}^1A'' \leftarrow \tilde{X}^1A'$ absorption spectra of HSiCl and DSiCl, the relative intensity of each vibrational component was expressed as the corresponding computed anharmonic FC factor multiplied by a frequency factor of power one, and a Gaussian line shape with a fwhm of 10 cm^{-1}. In all spectral simulations carried out, the experimental adiabatic relative electronic energies (including zero-point energy corrections) between the $\tilde{X}^1A'$ and $\tilde{A}^1A''$ states {i.e., the T_0 values of the $\tilde{A}^1A''$ state of HSiCl (20717.769 cm^{-1}) or DSiCl (20773.431 cm^{-1}) obtained from the LIF spectra[1]} were used for the sake of making direct comparison between simulated and observed spectra easier. Similarly, the wavenumber scale in each simulated SVL emission spectrum is taken relative to the laser excitation line, giving a direct measure of the ground electronic state vibrational energy, as normally used in published experimental dispersed fluorescence spectra.[2]

Results and Discussion

The optimized geometrical parameters, computed vibrational frequencies, and relative electronic energies of the $\tilde{X}^1A'$ and $\tilde{A}^1A''$ states of HSiCl obtained from the present investigation are summarized and compared with previously calculated or available experimental values in Tables 1−3. In Table 4, some of the computed anharmonic vibrational energies of the $\tilde{X}^1A'$ state of HSiCl and DSiCl obtained from variational calculations in the present work are compared with available experimental values from ref 2 (EPAPS Supporting Information[25]). In addition, some computed excitation energies from the $\tilde{X}^1A'(0,0,0)$ level to various vibrational levels of the $\tilde{A}^1A''$ state of HSiCl and DSiCl, corresponding computed FC factors and upper vibrational state assignments obtained from the FC factor calculations of the present study are compared with available experimental transition energies given in the LIF study of ref 1 in Tables 5 and 6. Calculated and experimental transition energies of some "hot" bands are also compared in these two tables. The fitted RCCSD(T)/AV5Z and CASSCF/MRCI+D/AV5Z PEFs of the $\tilde{X}^1A'$ and $\tilde{A}^1A''$ state of HSiCl have root-mean-square (rms) deviations of 9.4 and 23.1 cm^{-1}, respectively, from the computed *ab initio* energy data points, and the C_{ijk} values of the polynomials are given in Table 7. The rms deviation of the PEF of the $\tilde{A}^1A''$ state is relatively large, when compared with that of the $\tilde{X}^1A'$ state. This is mainly because considerably more energy points and wider ranges of the geometrical parameters were employed in the fitting (cf., those of the $\tilde{X}^1A'$ state) to make sure that the PEF is adequate for simulating the full absorption spectra of HSiCl and DSiCl, yet to be recorded. The full lists of the computed FC factors between the $\tilde{X}^1A'$ and $\tilde{A}^1A''$ states of HSiCl and DSiCl are available, upon request, from the authors.

Table 1. Computed Geometrical Parameters (in Å and deg) and Vibrational Frequencies {ω_1 (HSi), ω_2 (Bending), and ω_3 (SiCl) in cm^{-1}} of the $\tilde{X}^1A'$ State of HSiCl Obtained at Different Levels of Calculations

methods	r_e(HSi)	r_e(SiCl)	θ_e	ω_1	ω_2	ω_3
CAS/MRCI/AVQZ[a]	1.5085	2.0716	95.918			
CAS/MRCI+D[b]/AVQZ[a]	1.5158	2.0756	95.462			
CCSD(T)/AVQZ[a]	1.5184	2.0792	95.215	2054.1	818.6	524.2
CAS/MRCI+D[b]/ACVQZ[c]	1.5144	2.0461	97.479			
CCSD(T)/ACVQZ[c] (fc)	1.5178	2.0778	95.233			
CCSD(T)/ACVQZ[c]	1.5144	2.0715	95.183			
CAS/MRCI/AV5Z[d]	1.5081	2.0693	95.932			
CAS/MRCI+D[b]/AV5Z[d]	1.5154	2.0730	95.480			
CCSD(T)/AV5Z[d]	1.5180	2.0768	95.046			
CCSD(T)/AV5Z[d] PEF	1.5181	2.0767	95.059	2051.0	820.9	527.1
PEF (ν's)				1973.1	805.5	521.8
PEF (ω's; DSi^{35}Cl)				1476.4	600.3	522.3
PEF (ν's; DSi^{35}Cl)				1436.5	592.2	517.1
CBS1[e]	−0.0002	−0.0012	−0.085			
CBS2[f]	−0.0004	−0.0025	−0.177			
Core1[g]	−0.0040	−0.0077	−0.032			
Core2[h]	−0.0034	−0.0063	−0.050			
(CBS+Core)$_{lower}$[i]	1.5136	2.0666	94.819			
(CBS+Core)$_{upper}$[j]	1.5144	2.0693	94.930			
best theoretical r_e values[k]	1.514(1)	2.068(1)	94.9(1)			
B3LYP/6−311G(3df,3pd)[l]	1.5256	2.0968	94.8			
QCISD/6−311+G(3df,3pd)[l]	1.515	2.083	95.3			
CCSD(T)/cc-pCVTZ[m]	1.5187	2.0808	95.449	2044.6	821.7	529.8
CCSD(T)/cc-pCVQZ[m]	1.5138	2.0697	95.302			
empirical cc-pCVTZ[m] (r_e, ν's)	1.5140	2.0724	94.66	1964.60	808.56	528.18
CCSD(T)/cc-pV(Q+d)Z[n]	1.5180	2.0778				
CCSD(T)/cc-pwCVQZ[n]	1.5140	2.0700				
CCSD(T)/cc-pCVQZ[n]	1.5147	2.0700	95.303			
absorption[o] (r_0, ν's)	1.561	2.064	102.8		808	522
LIF[p] (r_e^z, ν's)	1.525(5)	2.067(3)	96.9(5)	1968.7(4)	805.9(2)	522.8(1)
DF[l] (ν's)				1968.8	805.9	522.8
DF[l] (r_z, ω^0's)	1.5275(10)	2.0747(2)	94.97(11)	2002.2(7)	809.5(2)	525.1(4)
DF[l] (r_e^z, ω's)	1.515(2)	2.0700(3)	95.0(1)	2044(1)	822(1)	529(1)
DF[l] (ν's; DSi^{35}Cl)				1434.4	592.3	518.1
DF[l] (ω^0's; DSi^{35}Cl)				1452(1)	595.1(1)	521.2(5)
DF[l] (ω's; DSi^{35}Cl)				1473.2(10)	601.3(10)	525.3(10)

[a] The aug-cc-pV(Q+d)Z basis set was used for Si and Cl. [b] MRCI energies plus Davidson corrections. [c] The aug-cc-pwCVQZ basis set was used for Si and Cl, and their $2s^22p^6$ electrons were correlated except when specified with (fc); see text. [d] The aug-cc-pV(5+d)Z basis set was used for Si and Cl. [e] The correction of extrapolation to the complete basis set (CBS) limit takes half of the difference between the computed CCSD(T) values obtained using the AVQZ and AV5Z basis sets; see text. [f] The correction of extrapolation to the complete basis set (CBS) limit employs the $1/X^3$formula using the computed CCSD(T) values obtained with the AVQZ and AV5Z basis sets; see text. [g] The correction of core electron correlation contribution to the computed geometrical parameters takes the difference between the computed CCSD(T) values obtained using the AVQZ (with the default frozen core) and ACVQZ {frozen only the Si and Cl $1s^2$ electrons} basis sets. [h] The correction of core electron correlation contribution to the computed geometrical parameters takes the difference between the computed CCSD(T) values obtained using the ACVQZ basis set with and without the $2s^22p^6$ electrons of Si and Cl being correlated in the CCSD(T) calculations. [i] Assuming that the basis set extrapolation and core electron correlation contributions are additive, this combination of the CBS and core corrections gives the lower limit of the combined contribution. [j] Assuming that the basis set extrapolation and core electron correlation contributions are additive, this combination of the CBS and core corrections gives the upper limit of the combined contribution. [k] The best theoretical estimates take the averaged value of the upper and lower limits (see footnotes i and j) and the uncertainties are the differences between the best estimates and the upper/lower limits. [l] From ref 2. [m] From ref 5. [n] From ref 6. [o] From ref 28. [p] From ref 1.

Optimized Geometrical Parameters, Computed Vibrational Frequencies, and Relative Electronic Energies. Considering the computed equilibrium bond lengths, r_e(HSi) and r_e(SiCl), and bond angle, θ_e(HSiCl), of the $\tilde{X}^1A'$ state of HSiCl, it can be seen from Table 1 that, RCCSD(T) values obtained previously (note that only relatively high level results are considered and included in Table 1) and from the present study using different basis sets or frozen cores agree very well. Specifically, the maximum differences in computed RCCSD(T) r_e(HSi), r_e(SiCl), and θ_e(HSiCl) values are smaller than 0.005 Å, 0.011 Å, and 0.5°, respectively. When the computed RCCSD(T) geometrical parameters of the $\tilde{X}^1A'$ state obtained using augmented basis sets in the present study are considered (previous calculations[5,6] did not use augmented basis sets; see Table 1), the ranges of the computed values are even narrower (within 0.0036 Å, 0.0077 Å, and 0.19°, respectively). However, computed CASSCF/MRCI and CASSCF/MRCI+D geometrical parameters of the $\tilde{X}^1A'$ state cover wider ranges of values. In particular, the computed CASSCF/MRCI+D/ACVQZ bond angle of 97.48° is larger than all other computed bond angles by ∼2°. Because the multireference character is not important for the $\tilde{X}^1A'$ state, as mentioned above, the RCCSD(T) results should be more reliable than the CASSCF/MRCI+D results. Consequently, contributions from extrapolation to the CBS limit and core correlation were estimated based only on the RCCSD(T) results, as shown in Table 1 (see footnotes e to k of Table

Table 2. Computed Geometrical Parameters (in Å and deg) and Vibrational Frequencies {ω_1 (HSi), ω_2 (Bending), and ω_3 (SiCl) in cm^{-1}} of the $\tilde{A}^1A''$ states of HSiCl Obtained at Different Levels of Calculations

methods	r_e(HSi)	r_e(SiCl)	θ_e	ω_1	ω_2	ω_3
CAS/MRCI/AVQZ[a]	1.5110	2.0506	117.957			
CAS/MRCI+D[b]/AVQZ[a]	1.5090	2.0505	117.931			
CAS/MRCI+D/ACVQZ[c] (fc)	1.5083	2.0491	117.964			
CAS/MRCI+D[b]/ACVQZ[c]	1.5046	2.0451	118.137			
CAS/MRCI/AV5Z[d]	1.5107	2.0480	117.939			
CAS/MRCI+D[b]/AV5Z[d]	1.5086	2.0476	117.909			
CAS/MRCI+D[b]/AV5Z[d] PEF	1.5083	2.0476	117.722	1962.2	594.0	536.4
PEF (ν's)				1771.1	569.2	527.0
PEF (ω's; $DSi^{35}Cl$)				1413.0	426.9	545.0
PEF (ν's; $DSi^{35}Cl$)				1318.0	414.1	537.7
CBS1[e]	−0.0002	−0.0015	−0.011			
CBS2[f]	−0.0004	−0.0030	−0.023			
Core1[g]	−0.0044	−0.0054	+0.206			
Core2[h]	−0.0037	−0.0040	+0.173			
$(CBS+Core)_{lower}$[i]	1.5038	2.0392	118.059			
$(CBS+Core)_{upper}$[j]	1.5047	2.0422	118.104			
best theoretical r_e values[k]	1.504(1)	2.041(2)	118.1(1)			
B3LYP/6−311G(3df,3pd)[l]	1.5012	2.066	115.5			
absorption[m] (r_0, ν's)	1.499	2.047	116.1	1250; 1756	568	533
LIF[n] (r_s, ν's)	1.511(9)	2.051(11)	116.3(3)	1747.08	563.87	532.32
LIF[n] (r_z, ω^0's)	1.548(7)	2.045(1)	118.1(4)	1839.6(5)	567.6(2)	534.8(2)
LIF[n] (r_e^z, ω's)	1.532(8)	2.040(3)	118.1(5)	1956.4	585.8	540.9
LIF[n] (ν's; $DSi^{35}Cl$)				1300.799	408.649	543.169
LIF[n] (ω^0's; $DSi^{35}Cl$)				1351.0(3)	409.5(2)	546.1(2)
LIF[n] (ω's; $DSi^{35}Cl$)				1408.3	418.2	552.2

[a] The aug-cc-pV(Q+d)Z basis set was used for Si and Cl. [b] MRCI energies plus Davidson corrections. [c] The aug-cc-pwCVQZ basis set was used for Si and Cl, and their $2s^22p^6$ electrons were correlated except when specified with (fc); see text. [d] The aug-cc-pV(5+d)Z basis set was used for Si and Cl. [e] The correction of extrapolation to the complete basis set (CBS) limit takes half of the difference between the computed MRCI+D values obtained using the AVQZ and AV5Z basis sets; see text. [f] The correction of extrapolation to the complete basis set (CBS) limit employs the $1/X^3$ formula using the computed MRCI+D values obtained with the AVQZ and AV5Z basis sets; see text. [g] The correction of core electron correlation contribution to the computed geometrical parameters takes the difference between the computed MRCI+D values obtained using the AVQZ (with the default frozen core) and ACVQZ {frozen only the Si and Cl $1s^2$ electrons} basis sets; see text. [h] The correction of core electron correlation contribution to the computed geometrical parameters takes the difference between the computed MRCI+D values obtained using the ACVQZ basis set with and without the $2s^22p^6$ electrons of Si and Cl being correlated in the CASSCF/MRCI+D calculations. [i] Assuming that the basis set extrapolation and core electron correlation contributions are additive, this combination of the CBS and core corrections gives the lower limit of the combined contribution. [j] Assuming that the basis set extrapolation and core electron correlation contributions are additive, this combination of the CBS and core corrections gives the upper limit of the combined contribution. [k] The best theoretical estimates take the averaged value of the upper and lower limits (see footnotes i and j) and the uncertainties are the differences between the best estimates and the upper/lower limits. [l] From ref 2. [m] From ref 28. [n] From ref 1.

1 for the methods employed to obtain the best theoretical estimates and their uncertainties). It can be seen that these contributions (Core1, Core2, CBS1, and CBS2 in Table 1) are generally quite small. The best estimated theoretical geometrical parameters of the $\tilde{X}^1A'$ state of HSiCl have $r_e(HSi) = 1.514 \pm 0.001$ Å, $r_e(SiCl) = 2.068 \pm 0.001$ Å, and $\theta_e = 94.9 \pm 0.1°$. These values agree very well with the "empirical cc-pCVTZ" values of 1.5140 Å, 2.0724 Å, and 94.66° (see Table 1) obtained previously[5] and also with the latest, estimated experimental r_e^z values of 1.515 ± 0.002 Å, 2.0700 ± 0.0003 Å, and $95.0 \pm 0.1°$ reported in the dispersed fluorescence study.[2] The "empirical cc-pCVTZ" r_e bond lengths and bond angle (see Table 1) were derived from equilibrium rotational constants obtained based on r_0 rotational constants (A_0, B_0, and C_0 from ref 1) corrected for vibrational effects employing centrifugal distortion and vibration−rotation constants derived from calculated harmonic and cubic force fields at the CCSD(T)/cc-pCVTZ level (see ref 5 for details).

For the $\tilde{A}^1A''$ state of HSiCl, the computed CASSCF/MRCI and CASSCF/MRCI+D geometrical parameters obtained using different basis sets or frozen cores are very consistent (see Table 2), unlike what was obtained for the $\tilde{X}^1A'$ state, as mentioned above. Moreover, similar to the $\tilde{X}^1A'$ state, contributions from extrapolation to the CBS limit and core correlation based on the more reliable CASSCF/MRCI+D values (c.f., the CASSCF/MRCI values without Davidson corrections; see Table 2) are generally small. The best estimated theoretical geometrical parameters obtained (see footnotes e to k of Table 2) have $r_e(HSi) = 1.504 \pm 0.001$ Å, $r_e(SiCl) = 2.041 \pm 0.002$ Å, and $\theta_e = 118.1 \pm 0.1°$. When these values are compared with the only previously computed values of ref 2, the B3LYP bond angle of 115.5° is clearly too small (see Table 2). If the the best estimated theoretical values obtained here are compared with the experimental r_e^z (estimated equilibrium) values of $r_e(HSi) = 1.532 \pm 0.008$ Å, $r_e(SiCl) = 2.040 \pm 0.003$ Å, and $\theta_e = 118.1 \pm 0.5°$ derived in the LIF study of ref 1, the agreement of within 0.001 Å and 0.1° for $r_e(SiCl)$ and θ_e is very good. However, the agreement for $r_e(HSi)$ is not as good, with the experimental $r_e^z(HSi)$ value larger than the best estimated theoretical value by 0.028 Å. Of particular relevance to the present study, the estimated experimental $r_e^z(HSi)$ values increase upon excitation from the $\tilde{X}^1A'$ to $\tilde{A}^1A''$ state (as derived from the dispersed fluorescence and LIF studies of refs 2 and 1, respectively; see Tables 1and 2), but the corresponding best estimated theoretical values obtained here decrease upon excitation. Nevertheless, the experimental

uncertainty of 0.008 Å given in ref 1 for the estimated equilibrium r_e^z(HSi) value of the $\tilde{A}^1A''$ state of HSiCl is significantly larger than that estimated for r_e^z(SiCl). In addition, the experimentally derived r_0(HSi) values of the $\tilde{X}^1A'$ and $\tilde{A}^1A''$ states of HSiCl (1.5214 ± 0.0008 Å and 1.505 ± 0.005 Å, respectively) reported in the LIF study[1] actually give a decrease in the r_0(HSi) bond length upon excitation. Similarly, the derived $r_0°$ and r_s HSi bond lengths also give decreases upon excitation (see ref 1 for details). It is only after including harmonic contributions, based on normal coordinate analysis and harmonic force fields, to obtain the r_z and r_e^z geometrical parameters that increases in the HSi bond length upon excitation are obtained. These increases are mainly because the r_z and r_e^z HSi bond lengths of the $\tilde{A}^1A''$ state become significantly larger than the r_0 and r_s values. It was noted in ref 1 that available data used in deriving the harmonic force fields were insufficient to determine some interaction force constants, which were assumed to be 0.0 in the fitting (see ref 1 for details). This may be the cause of the discrepancy between the best estimated theoretical r_e(HSi) bond length of the $\tilde{A}^1A''$ state of HSiCl obtained here and the experimental r_e^z value reported in ref 1. In any case, the best estimated theoretical r_e(HSi) value of the $\tilde{A}^1A''$ state of HSiCl agrees very well with the experimentally derived r_0 and r_s values of 1.505 ± 0.005 and 1.511 ± 0.009 Å, respectively, given in ref 1.

Regarding computed vibrational frequencies of the $\tilde{X}^1A'$ state of HSiCl, the differences between the computed harmonic values obtained using the AVQZ (numerical second derivative calculations) and AV5Z (variational calculations using the PEF) basis sets obtained in the present study are less than 4 cm^{-1} for all three vibrational modes (see Table 1). Comparing the computed fundamental frequencies of all three vibrational modes of the $\tilde{X}^1A'$ states of both HSiCl and DSiCl obtained here employing the RCCSD(T)/AV5Z PEF with the corresponding experimental values obtained from the dispersed fluorescence study,[2] the maximum discrepancy is less than 5 cm^{-1}. For the harmonic frequencies, the maximum difference between computed and experimentally derived values is 7 cm^{-1} for ω_1'', the HSi stretching mode, of HSiCl. Summing up, the agreement between theory and experiment is very good for the vibrational frequencies of the $\tilde{X}^1A'$ states of both HSiCl and DSiCl, suggesting that the RCCSD(T)/AV5Z PEF is highly reliable, particularly near the bottom of the potential energy well. For the $\tilde{A}^1A''$ state of HSiCl and DSiCl, the agreement between theory and experiment for the vibrational frequencies of the bending and SiCl stretching modes is within 10 cm^{-1} (see Table 2), which is reasonably good. For the HSi stretching mode, the computed ν_1' of HSiCl (1771.1 cm^{-1}; see Table 2) is larger than the experimental value (1747.08 cm^{-1}) by ~24 cm^{-1}, which is the largest discrepancy between computed and experimental vibrational frequencies of the $\tilde{A}^1A''$ states of HSiCl and DSiCl. Nevertheless, the computed and experimentally derived ω_1' values of the $\tilde{A}^1A''$ state of HSiCl agree to within 6 cm^{-1}. In addition, for the DSi stretching mode, the computed ν_1' value agree with the experimental value to within 18 cm^{-1}. It should be noted that the difference between the harmonic and fundamental frequencies of the HSi stretch mode is quite large (~200 cm^{-1} whether based on the computed or experimentally derived values; see Table 2), indicating large anharmonic effects. Employing linear combinations of harmonic basis functions for anharmonic vibrational wave functions may be inadequate for the HSi stretching mode of HSiCl.

Computed adiabatic electronic energies, T_e, of the $\tilde{A}^1A''$ state (relative to the $\tilde{X}^1A'$ state) of HSiCl obtained at different levels of calculation are summarized in Table 3. It can be seen that contributions from basis set extrapolation (CBS1 and CBS2 in Table 3) to the computed T_e values are very small (<0.0005 eV). However, core correlation contributions are significant (ca., −0.07 eV). The best estimated theoretical T_e value is 2.564 ± 0.067 eV (20683 ± 538 cm^{-1}). Including correction of zero-point vibrational energies of the two states involved (ΔZPE in Table 3), the best theoretical T_0 value is 2.54 ± 0.07 eV (20456 ± 560 cm^{-1}). It is pleasing that this value agrees with the experimental value of 2.5687 eV (20717.769 cm^{-1}) obtained from the LIF study[1] to within 0.03 eV (262 cm^{-1}). The best theoretical T_0 value of the $\tilde{A}^1A''$ state of DSiCl has also been estimated and given in Table 3, and it agrees with the experimental value also to within 0.03 eV (236 cm^{-1}). In summary, the *ab initio* results obtained in the present study agree very well with available experimental values.

Computed FC Factors and Simulated Absorption and SVL Emission Spectra. Before the simulated spectra are discussed, some computed and experimental vibrational energies of the $\tilde{X}^1A'$ state of HSiCl and DSiCl are compared in Table 4 (the form of the vibrational designations used follows those given in refs 2 and 25). It can be seen that agreements between computed and experimental energies are reasonably good, particularly for low-lying vibrational levels. Therefore, on energy grounds, all the vibrational assignments given in the dispersed fluorescence study[2] for the $\tilde{X}^1A'$ state of HSiCl and DSiCl are confirmed. Nevertheless, for a few vibrational levels, there are other vibrational levels, which are very close in energy according to our variational calculations of anharmonic vibrational wave functions of the $\tilde{X}^1A'$ states of HSiCl and DSiCl, and hence, alternative assignments are possible based on our computed anharmonic vibrational energies. These are the 1_12_7 level of HSiCl and the 2_{11} and 2_{12} levels of DSiCl (as shown with two energy entries under "calcd" in Table 4). However, for these relatively high energy vibrational levels with high quantum numbers in the bending mode (ν_2''), the computed anharmonic vibrational wave functions are rather mixed with no single dominant harmonic basis functions. This is also the case for high vibrational levels of the $\tilde{A}^1A''$ state to be discussed below, particularly for HSiCl, where ν_2' and ν_3' are close in energy {difference 31.55 (experimental value) and 42.3 (computed value) cm^{-1}} and their normal modes show mixing of bending and SiCl stretching. For some of these levels, which are heavily mixed, the vibrational designations have been determined based on both the computed anharmonic vibrational wave functions and the expected vibrational spacing of a series, and they may be tentative.

Table 3. Computed Relative Electronic Energies in eV (cm^{-1}) between the $\tilde{X}^1A'$ and $\tilde{A}^1A''$ States of HSiCl Obtained at Different Levels of Calculations

method[a]	T_e
CASSCF/MRCI/AVQZ[b]	2.6602 (21456.3)
CASSCF/MRCI+D/AVQZ[b]	2.6306 (21217.4)
CASSCF/MRCI+D/ACVQZ[b] (fc)	2.6291 (21205.3)
CASSCF/MRCI+D/AVCQZ[c]	2.5488 (20557.1)
CASSCF/MRCI+D/AVCQZ[b]	2.5628 (20670.2)
CASSCF/MRCI/AV5Z[b]	2.6533 (21400.3)
CASSCF/MRCI+D/AV5Z[b]	2.6311 (21220.9)
CBS1[d]	+0.00022 (+1.8)
CBS2[e]	+0.00047 (+3.7)
Core1[f]	−0.06782 (−547.0)
Core2[g]	−0.06634 (−535.1)
$(CBS+Core)_{lower}$[h]	2.5635 (20675.7)
$(CBS+Core)_{upper}$[i]	2.5652 (20689.5)
best theoretical T_e value[j]	2.564 ± 0.067 (20683 ± 538)
ΔZPE correction[k]	−0.02815 (−227.07)
best theoretical T_0 value[l]	2.54 ± 0.07 (20456 ± 560)
ΔZPE correction[k]	−0.01811 (−146.09)
best theoretical T_0 value[l] (DSiCl)	2.55 ± 0.07 (20537 ± 560)
absorption[m] T_0	2.5687 (20717.65)
LIF[n] T_0	2.5687 (20717.769)
LIF[n] T_0 ($DSi^{35}Cl$)	2.5756 (20773.431)

[a] For the basis set used, see footnotes of Table 1. [b] At the corresponding optimized geometries. [c] The $\tilde{X}^1A'$state CASSCF/MRCI+D/ACVQZ energy was computed at the $\tilde{X}^1A'$ CCSD(T)/AVQZ optimized geometry, because the computed θ_e value of the $\tilde{X}^1A'$ state obtained at the CASSCF/MRCI/ACVQZ level is significantly larger than values obtained with the RCCSD(T) method. It can be seen that this geometry effect on the computed T_e value is small (0.014 eV). [d] The correction of extrapolation to the complete basis set (CBS) limit takes half of the difference between the computed MRCI+D values obtained using the AVQZ and AV5Z basis sets; see text. [e] The correction of extrapolation to the complete basis set (CBS) limit employs the $1/X^3$ formula using the computed MRCI+D values obtained with the AVQZ and AV5Z basis sets; see text. [f] The correction of core electron correlation takes the difference between the computed MRCI+D values obtained using the AVQZ (with the default frozen core) and ACVQZ {frozen only the Si and Cl $1s^2$ electrons} basis sets; see text. [g] The correction of core electron correlation takes the difference between the computed MRCI+D values obtained using the ACVQZ basis set with and without the $2s^22p^6$ electrons of Si and Cl being correlated in the CASSCF/MRCI+D calculations. [h] Assuming that the basis set extrapolation and core electron correlation contributions are additive, this combination of the CBS and core corrections gives the lower limit of the combined contribution. [i] Assuming that the basis set extrapolation and core electron correlation contributions are additive, this combination of the CBS and core corrections gives the upper limit of the combined contribution. [j] The best theoretical estimate takes the averaged value of the upper and lower limits (see footnotes h and i) and the uncertainty is the difference between the best estimate and the MRCI+D/AVQZ value (in view of the rather large core correlation contributions; see text). [k] The zero-point vibrational energy correction has employed experimental fundamental vibrational frequencies of the two states from refs 1 and 2, respectively. [l] $T_0 = T_e + \Delta ZPE$. [m] From ref 28. [n] From ref 1.

Computed (E_{calcd} in Table 5) and experimental (E_{exptl}; from the LIF study of ref 1) excitation energies from the $\tilde{X}^1A'(0,0,0)$ level to the $\tilde{A}^1A''(v_1',v_2',v_3')$ levels of HSiCl and also excitation energies of some "hot" bands, with their corresponding computed FC factors (computed at a Boltzmann vibrational temperature of 300 K), are compared in Table 5. Some possible alternative assignments to those given in the LIF study are also given in Table 5, on the basis of the computed FC factors and anharmonic vibrational energies. These alternative assignments are mainly for transitions, where the discrepancies between the computed and experimental energies are larger than ~20 cm^{-1}, the experimental vibrational spacings differ significantly from what would be expected for the assigned progression or the computed FC factors with the assignments of ref 1 are relatively small. For example, for the $\tilde{A}^1A''(1,v_2',0)''$ $\tilde{X}^1A'(0,0,0)$ progression (with $v_2' = 1-4$; based on the assignments of the LIF study), the experimental transition energies are smaller than the corresponding computed energies by over 60−145 cm^{-1} (see Table 5). In addition, the experimental vibrational spacings of between ~498 and 463 cm^{-1} are significantly smaller than the corresponding computed values of between 538 and 498 cm^{-1}. The latter, larger computed vibrational spacings are reasonable for a progression involving the bending mode, which has a ν_2' value of 569.2 (computed value) or 563.87 (experimental value; see Table 2) cm^{-1}. In this connection, the experimental spacings seem to be too small for a vibrational progression involving ν_2'. Consequently, alternative assignments based on computed transition energies were found for these observed vibrational components. Most of the alternative assignments shown in Table 5 give better agreement between the computed and experimental transition energies, more reasonable vibrational spacings between the vibrational components concerned, or larger computed FC factors than those computed for the original assignments given in the LIF study.[1] Nevertheless, some alternative assignments also give possible weaker overlapping vibrational components (vide infra).

Similar to that shown in Table 5, computed (E_{calcd}) and experimental (E_{exptl}) excitation energies from the $\tilde{X}^1A'(0,0,0)$ level to various $\tilde{A}^1A''(v_1',v_2',v_3')$ levels of DSiCl and also excitation energies of some hot bands are compared in Table 6. Some possible alternative assignments are also included in the table, based on what has been discussed above for Table 5. For both HSiCl and DSiCl, it appears that most of the vibrational assignments of combination bands involving the HSi or DSi stretching mode given in ref 1 must be revised on the basis of the results of FC calculations carried out in the present investigation. In addition, hot bands arising from the excited vibrational level of the $\tilde{X}^1A'$ states of HSiCl and DSiCl with $v_1'' = 1$ (see Tables 5 and 6) have small computed FC factors at a Boltzmann vibrational temperature of 300 K, because ν_1'' has a relatively large value {1968.8 and 1434.4 cm^{-1} for HSiCl and DSiCl, respectively (experimental values; see Table 1); cf. the other two vibrational modes}. Consequently, alternative assignments with larger computed FC factors at similar transition energies were found for these observed vibrational components, assigned to hot bands arising from excited vibrational levels with $v_1'' = 1$ in ref 1. However, it should be noted that a Boltzmann vibrational temperature of 300 K has been assumed in the FC factor calculations. HSiCl or DSiCl molecules produced in an electric discharge of $SiHCl_3$ or $SiDCl_3$, respectively, diluted in Ar through a pulsed jet[1] may have a vibrational temperature higher than 300 K or may be excited preferentially in the HSi or DSi stretching modes (i.e., with a non-Boltzmann distribution). Because in their formation, there

Table 4. Computed Vibrational Energies (cm^{-1}) of the $\tilde{X}^1A'$ State of HSiCl and DSiCl and Their Assignments and the Corresponding Experimental Values[25] from the SVL Emission (DF, Dispersed Fluorescence) Study of Ref 2

	HSiCl		DSiCl	
assignment	DF	calcd	DF	Calcd
1_1	1968.8	1973.1	1434.4	1436.5
1_2	3870.1	3879.3	2832.9	2837.5
2_1	805.9	805.5	592.3	592.2
2_2	1607.7	1604.9	1183.6	1180.8
2_3	2400.7	2398.5	1769.0	1765.9
2_4	3190.9	3186.7	2354.4	2347.7
2_5	3977.5	3969.6	2932.6	2926.2
2_6	4755.5	4747.3	3509.2	3501.7
2_7	5526.4	5519.8	4082.7	4074.0
2_8	6292.6	6287.6	4652.2	4643.6
2_9			5217.7	5210.5
2_{10}			5781.6	5776.0
2_{11}			6338.0	6336.6; 6343.4
2_{12}			6893.3	6881.1; 6913.8
3_1	522.8	521.8	518.1	517.1
3_2	1037.9	1039.7	1031.2	1030.4
3_3	1553.5	1553.5		
3_4	2061.5	2063.4		
1_12_1	2758.7	2763.9	2020.3	2021.8
1_12_2	3543.6	3548.5	2603.4	2605.3
1_12_3	4324.9	4327.5	3184.3	3184.2
1_12_4	5100.9	5101.1	3759.0	3759.7
1_12_5	5865.5	5869.4	4333.6	4331.7
1_12_6	6628.6	6633.0	4901.6	4900.7
1_12_7	7384.4	7381.8; 7393.2	5466.6	5466.7
1_12_8			6029.6	6030.3
1_13_1	2491.4	2495.9	1952.1	1953.3
1_23_1	4390.4	4403.0		
2_13_1	1324.8	1323.9	1109.4	1107.0
2_23_1	2125.0	2119.9	1698.3	1693.2
2_33_1	2914.8	2910.4	2280.7	2276.1
2_43_1	3700.9	3695.7	2863.6	2855.6
2_53_1	4458.0	4475.8	3439.2	3432.1
2_63_1	5260.0	5250.9	4016.3	4005.5
2_73_1	6027.2	6021.4	4584.7	4576.0
2_83_1	6787.0	6788.9	5154.1	5143.9
2_93_1	7546.3	7557.8	5717.0	5710.6
$2_{10}3_1$			6279.4	6279.2
$2_{11}3_1$			6835.8	6834.1
2_13_2	1841.3	1838.2	1622.1	1617.8
2_23_2	2634.9	2631.0	2205.3	2201.8
2_33_2	3423.6	3418.3	2786.4	2782.4
2_43_2	4206.3	4200.6	3365.8	3359.8
2_53_2	4987.3	4978.0	-	
2_63_2	5757.3	5750.9	4512.3	4505.5
2_73_2	6522.3	6520.5	5081.1	5074.5
2_83_2			5647.6	5642.2
2_93_2			6211.7	6210.4
$2_{10}3_2$			6770.4	6773.9
2_13_3	2349.6	2348.6		
2_23_3	3141.8	3138.0		
2_33_3	3926.3	3922.3		
2_43_3	4706.0	4701.6	3864.8	3860.1
2_53_3	5484.3	5476.5	4438.2	4432.5
2_63_3			5008.1	5002.4
2_73_3			5574.8	5571.6
2_13_4	2855.2	2855.0		
2_23_4	3643.9	3641.1		
2_33_4	4425.8	4422.3		
2_43_4	5202.2	5199.0		
2_53_4	5974.2	5972.8		
$1_12_13_1$	3279.4	3283.0	2535.6	2537.1
$1_12_23_1$	4063.9	4064.3	3116.9	3117.2
$1_12_33_1$	4836.8	4840.1		
$1_12_43_1$	5608.2	5610.6	4271.9	4267.0
$1_12_53_1$	6374.0	6376.3	4837.2	4836.9
$1_12_63_1$	7134.0	7138.2		
$1_22_13_1$	5165.6	5174.5		
$1_22_23_1$	5931.9	5941.6		
$1_22_33_1$	6693.1	6704.1		
$1_22_43_1$	7449.6	7463.1		
$1_12_13_2$			3047.1	3047.5

is an increase in the HSi bond length from 1.464 Å {r_s(HSi) in $HSiCl_3$}[26] to 1.515 Å in HSiCl (r_e^z value from ref 2).

The simulated absorption spectra of HSiCl and DSiCl at a Boltzmann vibrational temperature of 300 K are shown in Figures 1 and 2, respectively. The assignments of some major vibrational progressions and some hot bands are also indicated in these figures. It can be seen that the main simulated vibrational progression is $\tilde{A}^1A''(0,v_2',0) \leftarrow \tilde{X}^1A'(0,0,0)$, involving the bending mode in the upper state of both HSiCl and DSiCl, as expected from the major geometry change in the bond angle (see Tables 1 and 2) upon excitation. Based on the computed FC factors, some combination bands involving ν_2' and ν_3' should be excited, particularly for HSiCl (Figure 1). The full simulated absorption spectra of HSiCl and DSiCl cover excitation energies in the range between ~20 000 and 26 000 cm^{-1}. The band maxima are at 21 837.25 and 22 384.08 cm^{-1} (experimental values; Tables 5 and 6) corresponding to the $\tilde{A}^1A''(0,2,0) \leftarrow \tilde{X}^1A'(0,0,0)$ and $\tilde{A}^1A''(0,4,0) \leftarrow \tilde{X}^1A'(0,0,0)$ vibrational components for HSiCl and DSiCl, respectively. In addition to the major vibrational progressions shown in Figures 1 and 2, there are a large number of minor combination bands and hot bands according to the FC factor calculations (the lists are available upon request from the authors).

A portion of the simulated absorption spectrum of HSiCl is compared with the corresponding portion of the experimental LIF spectrum[1] in Figure 3 (top and bottom traces, respectively). Computed relative FC factors in the same spectral region are also shown as a bar diagram in Figure 3 (middle) to show some vibrational components, which are very close in energy and hence cannot be resolved in the simulated spectrum with a fwhm of 10 cm^{-1}. It can be seen from Figure 3 that the agreement between the simulated absorption and experimental LIF spectra is reasonably good, bearing in mind the spread of the rotational structure and uncorrected intensity (frequency-dependent laser intensity and detector sensitivity) of the experimental spectrum and that the published experimental LIF spectrum may consist of different fragment portions recorded under different experimental conditions. In any case, the assignments of the main vibrational structure given by ref 1 are confirmed by our spectral simulation. However, the weak hot bands assigned to $1_1^12_0^1$ and $1_1^12_0^2$ in the experimental LIF spectrum have very small computed relative FC factors (0.003 and 0.004, with the maximum value set to 100; see Table 5) and hence do not appear in the simulated spectrum with a Boltzmann vibrational temperature of 300 K. Instead, the 2_1^2 and $2_1^13_0^1$ hot bands are found in the simulated absorption spectrum to be roughly in the position of the weak structure assigned to the $1_1^12_0^1$ hot band in the experimental LIF spectrum and to have more intensity (see also Table 5). In addition, computed FC factors (the bar diagram in the middle of Figure 3) suggest that there are some weak hot bands, namely 3_1^1, 3_1^2, $2_0^13_1^1$, $2_0^13_1^2$, and $2_0^23_1^1$, underneath the main 0_0^0, 3_0^1, 2_0^1, $2_0^13_0^1$, and 2_0^2 vibrational components, respectively (see also Table 5).

Portions of the simulated absorption and experimental LIF spectra of DSiCl are compared in Figure 4 (bottom and top traces). Similar to HSiCl discussed above, the general

Table 5. Computed (E_{calcd}) and Experimental (E_{exptl}; from ref 1) Excitation Energies (in cm^{-1}) from the $\tilde{X}^1A'(0,0,0)$ Vibronic Level to the $\tilde{A}^1A''(v_1',v_2',v_3')$ Levels of HSiCl, Some "Hot" Bands with the Computed Franck−Condon (FC) Factors, and Possible Alternative Assignments Based on the Computed FC factors and Anharmonic Vibrational Energies (See Text)

LIF		calculation	
(v_1',v_2',v_3')	E_{exptl}	E_{calcd} [FCF]	alternative assignments
(0,0,0)	20717.769	20717.769[a] [18.3]	20722.9 [1.5] 3_1^1
(1,0,0)	22464.85	22488.9 [0.1]	22422.1 [6.1] $2_0^4 3_1^0$; 22440.3 [0.4] $2_0^5 3_2^0$
(0,1,0)	21281.64	21287.0 [63.7]	21288.3 [3.7] $2_0^1 3_1^1$
(0,2,0)	21837.25	21848.0 [100.0]	21845.0 [3.1] $2_0^2 3_1^1$
(0,3,0)	22384.94	22400.4 [84.2]	
(0,4,0)	22925.27	22943.9 [33.5]	
(0,0,1)	21250.09	21244.8 [6.7]	21245. [0.9] 3_1^2
(0,0,2)	21777.89	21767.3 [1.2]	
(0,0,3)	22301.80	22285.4 [0.1]	
(0,0,4)	22819.76	22799.0 [0.005]	
(1,1,0)	22971.92	23032.9 [0.8]	23000.0 [1.0] (1,0,1); 22958.1 [3.7] $2_0^5 3_1^0$
(1,2,0)	23470.37	23571.2 [0.9]	23479.9 [4.2] (0,5,0)
(1,3,0)	23955.77	24064.7 [1.5]	23977.8 [0.8] (0,6,0)
(1,4,0)	24419.72	24564.2 [1.6]	24428.8 [0.2] (0,5,2)
(2,1,0)	24445.82	24534.0 [0.5]	24450.0 [0.1] (4,3,0)
(1,0,1)	23008.76	23000.0 [1.0]	
(1,0,2)	23547.89	23504,9 [2.7]	23535.0 [2.8] (1,1,1); 23542.9 [0.2] $1_0^1 2_0^3 3_1^0$
(1,0,3)	24081.38	24002.3 [4.7]	24064.7 [1.5] (1,3,0); 24069.6 [0.2] $1_0^1 2_0^1 3_1^3$
(2,0,1)	24527.72	24600.9 [0.03]	24520.0 [1.6] (1,1,3); 24519.8 [0.2] $1_0^1 3_1^5$
(0,1,1)	21808.75	21810.2 [30.1]	21807.6 [3.4] $2_0^1 3_1^2$
(0,2,1)	22357.40	22366.9 [57.7]	
(0,3,1)	22896.20	22913.3 [55.7]	
(0,4,1)	23427.25	23448.8 [18.6]	23421.9 [16.2] (0,3,2)
(0,1,2)	22331.55	22329.3 [6.3]	
(0,2,2)	22871.88	22882.0 [14.6]	
(0,3,2)	23399.93	23421.9 [16.2]	23393.5 [1.9] (0,2,3)
(0,1,3)	22849.84	22844.3 [0.6]	
(0,2,3)	23378.10	23393.5 [1.9]	23380.3 [0.3] $2_0^2 3_1^4$
(0,1,4)	23362.73	23355.4 [0.03]	
(1,1,1)	23508.38	23535.0 [2.8]	23504.9 [2.7] (1,0,2)
(1,2,1)	23999.81	24104.6 [0.3]	24002.3 [4.7] (1,0,3)
(1,3,1)	24479.14	24634.2 [0.03]	24489.4 [4.0] (1,0,4)
(1,1,2)	24039.56	24030.7 [3.9]	
1_1^1	20496.11	20515.8 [0.002]	20481.5 [2.0] 2_1^1
1_1^2	22023.31	22095.2 [0.0008]	22038.8 [0.015] $2_1^1 3_0^3$; 22031.5 [0.003] $2_1^1 3_1^4$
$1_1^1 2_0^1$	21003.21	21059.7 [0.003]	21004.7 [0.17] $2_1^1 3_0^1$; 21042.7 [1.0] 2_1^2
$1_1^1 2_0^2$	21501.55	21561.9 [0.004]	21523.8 [0.006] $2_1^1 3_0^2$
$1_1^1 2_0^3$	21986.95	22091.6 [0.0008]	21993.5 [0.0002] $2_1^0 3_0^4$
$1_1^1 3_0^1$	21040.03	21026.8 [0.003]	21042.5 [1.0] 2_1^2
$1_1^1 3_0^2$	21578.89	21561.9 [0.004]	21594.9 [0.006] 2_1^3; 21561.3 [0.003] $2_1^2 3_0^1$
$1_1^1 2_0^1 3_0^1$	21539.59	21531.7 [0.004]	21523.8 [0.006] $2_1^1 3_0^2$
$1_1^1 2_0^1 3_0^2$	22030.93	22029.1 [0.004]	21042.5 [1.0] 2_1^2; 21043.0 [0.03] $2_1^2 3_1^1$
2_1^0	19911.81	19912.3 [1.2]	
2_1^1	20475.66	20481.5 [2.0]	
$2_1^0 3_0^1$	20444.15	20439.3 [0.1]	20443.5 [0.02] $2_1^0 3_1^2$
$1_0^1 2_1^4$	23614.19	23828.8 [0.001]	23623.4 [0.08] $2_1^5 3_0^2$
$1_0^2 2_1^1$	23640.28	23728.5 [0.04]	23644.5 [0.07] $2_1^4 3_0^3$
$1_0^1 2_1^3 3_0^1$	23673.79	23683.9 [0.3]	
3_1^0	20194.95	20195.9 [0.03]	
$2_0^1 3_1^0$	20758.75	20765.2 [0.04]	
$2_0^2 3_1^0$	21314.45	21326.2 [1.1]	
$2_0^3 3_1^0$	21861.91	21878.6 [4.0]	
$2_0^4 3_1^0$	22402.45	22422.1 [6.0]	
3_1^1	20727.35	20722.9 [1.5]	
3_1^2	21255.11	21245.5 [0.9]	
3_1^4	22296.72	22277.2 [0.02]	
$1_0^1 2_0^1 3_1^0$	22449.06	22511.0 [0.008]	22422.1 [6.1] $2_0^4 3_1^0$
$1_0^1 2_0^2 3_1^0$	22947.41	23049.4 [0.08]	22958.1 [3.7] $2_0^5 3_1^0$
$1_0^1 3_1^1$	22485.95	22478.1 [0.004]	22488.9 [0.1] (1,0,0); 22489.6 [0.6] $2_0^5 3_1^1$
$1_0^1 3_1^2$	23024.83	22983.0 [0.04]	23032.9 [0.8] (1,1,0); 23049.4 [0.08] $1_0^1 2_0^2 3_1^0$
$2_0^1 3_1^1$	21285.93	21288.3 [3.7]	
$2_0^3 3_1^1$	22373.22	22391.4 [0.3]	
$1_0^1 2_0^1 3_1^1$	22985.56	23013.2 [0.01]	22971.8 [0.3] $2_0^6 3_2^0$; 22983.0 [0.04] $1_0^1 3_1^2$
$2_1^0 3_1^1$	19924.67	19920.9 [0.09]	19912.3 [1.2] 2_1^0

[a] Fixed to the experimental value.

agreement between theory and experiment is reasonably good, and most of the assignments of the main vibrational structure can be confirmed. However, the 3_0^2 and 1_0^1 vibrational components have very small computed FC factors (0.3 and 0.02, respectively; see Table 6) and hence are not observable in the simulated absorption spectrum (Figure 3 bottom trace). Nevertheless, such discrepancies between the simulated absorption and experimental spectra could be because the latter has not been corrected for frequency dependent intensity or because it consists of different portions

Table 6. Computed (E_{calcd}) and Experimental (E_{exptl}) Excitation Energies (in cm^{-1}) from the $\tilde{X}^1A'(0,0,0)$ Vibronic Level to the $\tilde{A}^1A''(v_1',v_2',v_3')$ Levels of DSiCl, Some "Hot" Bands, with the Computed Franck−Condon (FC) Factors, and Possible Alternative Assignments Based on the Computed FC factors and Anharmonic Vibrational Energies (See Text)

LIF		calculation	
(v_1',v_2',v_3')	E_{exptl}	E_{calcd} [FCF]	alternative assignments
(0,0,0)	20773.431	20773.431[a] [4.9]	
(1,0,0)	22074.23	22090.4 [0.02]	22061.2 [0.05] $2_1^2 3_0^2$
(0,1,0)	21182.08	21186.6 [23.7]	21203.9 [2.0] $2_0^1 3_1^1$
(0,2,0)	21587.19	21595.8 [57.6]	21609.9 [3.8] $2_0^2 3_1^1$
(0,3,0)	21988.07	22001.6 [90.5]	22012.3 [4.6] $2_0^3 3_1^1$
(0,4,0)	22384.08	22403.7 [100.0]	22411.0 [4.1] $2_0^4 3_1^1$
(0,5,0)	22774.51	22801.7 [78.8]	22775.6 [0.09] (0,1,3); 22805.8 [2.6] $2_0^5 3_1^1$
(0,6,0)	23158.20	23194.9 [42.3]	23156.6 [0.009] (1,0,2); 23197.6 [1.3] $2_0^6 3_1^1$
(0,7,0)	23533.85	23584.1 [13.3]	23545.5 [0.04] (1,1,2)
(0,8,0)	23899.33	23974.2 [1.1]	23881.2 [0.3] $2_0^9 3_1^0$; 23903.2 [0.06] $1_0^2 2_0^3 3_1^0$
(0,9,0)	24252.87	24369.4 [0.8]	24237.4 [0.07] (0,6,2); 24259.3 [0.01] $2_0^6 3_1^3$; 24263.3 [0.03] $1_0^2 2_0^4 3_1^0$
(0,10,0)	24591.74	24816.5 [0.3]	24571.4 [0.2] $1_0^1 2_1^0 3_0^8$
(0,0,1)	21316.60	21311.1 [2.0]	
(0,0,2)	21854.48	21844.1 [0.3]	21855.3 [0.08] 3_1^3
(1,1,0)	22464.33	22485.9 [0.3]	22460.2 [0.3] $2_1^2 3_0^3$
(1,2,0)	22849.09	22876.5 [1.4]	22855.8 [0.4] $2_1^2 3_0^4$
(1,3,0)	23228.62	23262.4 [3.9]	23194.9 [41.2] (0,6,0)
(1,4,0)	23601.73	23643.6 [6.4]	23584.1 [13.3] (0,7,0); 23591.4 [0.3] $2_0^7 3_1^1$
(1,5,0)	23966.83	24020.2 [6.6]	23974.2 [1.1] (0,8,0); 23951.1 [0.3] $1_0^1 2_1^5 3_0^1$
(1,6,0)	24321.72	24398.2 [2.4]	24309.3 [0.1] (1,3,2)
(1,7,0)	24663.59	24748.5 [0.8]	24686.8 [0.09] (1,4,2); 24646.5 [0.08] $1_0^1 2_0^8 3_1^0$
(2,1,0)	23641.52	23689.1 [0.00007]	23643.6 [6.4] (1,4,0)
(2,2,0)	24001.68	24056.6 [0.07]	24020.2 [6.6] (1,5,0)
(2,3,0)	24353.33	24420.3 [0.6]	24369.4 [0.8] (0,9,0); 24358.6 [0.1] $2_1^9 3_0^1$
(1,0,1)	22615.03	22625.9 [0.03]	22602.6 [3.0] 2_1^6
(0,1,1)	21722.07	21721.1 [8.7]	
(0,2,1)	22123.74	22127.0 [18.5]	
(0,3,1)	22521.05	22529.4 [24.1]	
(0,4,1)	22913.49	22928.1 [20.5]	
(0,5,1)	23299.85	23322.9 [11.2]	
(0,6,1)	23679.05	23714.7 [3.6]	23682.4 [0.001] (1,0,3); 23645.2 [0.1] $2_1^6 3_0^2$
(0,1,2)	22256.84	22250.7 [1.3]	
(0,2,2)	22655.04	22653.6 [2.2]	
(0,3,2)	23048.72	23052.4 [2.2]	
(0,4,2)	23437.17	23448.0 [1.3]	23448.2 [0.3] $2_0^4 3_1^3$
(1,1,1)	23001.42	23018.2 [0.2]	22991.8 [3.3] 2_1^7
(1,2,1)	23382.94	23405.4 [0.7]	23381.9 [1.5] 2_1^8
(1,3,1)	23758.63	23788.0 [1.3]	23777.2 [0.02] 2_1^9
(1,4,1)	24127.72	24166.4 [1.4]	24108.6 [0.5] (0,7,1)
(1,5,1)	24488.16	24543.3 [0.9]	24489.2 [0.04] $2_1^8 3_0^2$
(2,1,1)	24175.30	24219.1 [0.003]	24166.4 [1.8] (1,4,1); 24169.7 [0.2] $1_0^1 2_0^4 3_1^2$
(2,2,1)	24531.29	24583.5 [0.03]	24543.1 [0.9] (1,5,1);
(2,3,1)	24879.31	24943.3 [0.005]	24910.1 [0.1] (1,6,1)
(1,1,2)	23533.47	23545.5 [0.04]	
(1,2,2)	23911.09	23929.5 [0.1]	
(1,3,2)	24282.93	24309.3 [0.1]	
(1,4,2)	24647.50	24686.8 [0.09]	24646.5 [0.08] $1_0^1 2_0^8 3_1^0$
1_1^1	20640.08	20653.9 [0.006]	20669.4 [0.05] 2_1^1; 20614.1 [0.3] $2_1^1 3_1^1$
1_1^2	21841.02	21879.1 [0.0004]	21844.1 [0.3] (0,0,2); 21855.1 [0.08] 3_1^3
$1_1^1 2_0^1$	21029.73	21049.4 [0.03]	21020.1 [0.2] $2_1^2 3_1^1$
$1_1^1 2_0^2$	21414.9	21440.0 [0.07]	21409.3 [2.3] 2_1^3; 21422 [0.1] $2_1^3 3_1^1$
$1_1^1 2_0^3$	21794.18	21826.0 [0.1]	
$1_1^1 2_0^4$	22167.29	22207.1 [0.09]	22164.4 [0.04] $2_0^6 3_2^0$
$1_1^2 2_0^1$	22207.16	22252.6 [0.003]	22209.4 [0.8] 2_1^5; 22207.1 [0.09] $1_1^1 2_0^4$
$1_1^2 2_0^2$	22567.16	22620.1 [0.01]	22583.7 [0.04] $1_1^1 2_0^5$; 22582.7 [0.03] $2_1^2 3_0^3$
$1_1^2 2_0^3$	22919.06	22983.8 [0.03]	22928.1 [20.5] (0,4,1); 22930.9 [2.2] $2_0^4 3_1^2$
$1_1^1 2_0^2 3_0^1$	21948.52	21968.9 [0.01]	21937.2 [0.05] $2_1^3 3_0^1$
$1_1^1 2_0^3 3_0^1$	22324.00	22351.5 [0.02]	22335.9 [0.9] $2_1^4 3_0^1$
2_1^1	20589.41	20594.3 [3.5]	
2_1^2	20994.8	21003.6 [4.4]	
$2_0^2 3_1^0$	21069.1	21078.7 [0.004]	21069.9 [0.004] $2_2^1 3_0^2$
$2_0^3 3_1^0$	21470.0	21484.4 [0.4]	21472.6 [0.01] $2_2^2 3_0^2$
$2_0^2 3_1^1$	21605.65	21609.9 [3.8]	
$2_0^3 3_1^1$	22003.00	22012.3 [4.6]	
$2_0^1 3_1^2$	21728.62	21733.6 [1.3]	

[a] Fixed to the experimental value.

recorded under different experimental conditions, as mentioned above. Similar to HSiCl, computed FC factors suggest some contributions from weak hot bands to the main vibrational structure (see the bar diagram in the middle Figure 4), but they are so close in energy that they will not be resolved in the simulated spectrum with a fwhm of 10 cm^{-1}. Overall, it can be concluded that the agreement between the simulated absorption and experimental LIF spectra of HSiCl and DSiCl is good.

The simulated and experimental $\tilde{A}^1A''(0,0,0) \rightarrow \tilde{X}^1A'$ SVL emission spectra of HSiCl are compared in Figure 5 (top and second from top, respectively). It can be seen that the

Table 7. RCCSD(T)/aug-cc-pV5Z and CASSCF/MRCI+D/aug-cc-pV5Z PEFs of the $\tilde{X}^1A'$ and $\tilde{A}^1A''$ States of HSiCl {C_{ijk}; See Text and Eq *1*}

$(i,j,k)^a$	$\tilde{X}^1A'$	$\tilde{A}^1A''$
200	0.276297	0.252828
020	0.298425	0.312888
002	0.099921	0.049566
110	0.011694	−0.014379
101	−0.007743	0.014213
011	0.045098	0.014961
300	−0.425380	−0.494550
030	−0.453991	−0.507081
003	0.012296	−0.006902
210	0.014470	−0.005445
201	−0.000684	0.004654
120	−0.024499	−0.009130
021	−0.066495	−0.031292
102	−0.024798	−0.043138
012	−0.097468	−0.044741
111	−0.037525	−0.031976
400	0.440379	0.443721
040	0.483647	0.550709
004	0.027711	0.009272
310	−0.010392	0.006362
301	0.004372	−0.011545
130	0.022119	0.024504
031	0.035256	0.006376
103	−0.025911	0.010411
013	0.019163	0.013650
220	0.002746	0.021209
202	−0.033945	−0.034754
022	0.036571	0.012030
211	−0.003977	0.007443
121	0.050357	0.018099
112	0.024835	0.028248
050	−0.388735	−0.541210
060	0.155526	0.286202
005	0.040039	0.081228
006	0.048156	0.062328
500	−0.356954	−0.256333
600	0.159079	0.084583
β	−0.027306	−0.200886

[a] *i*, *j*, and *k* are subscripts (indices) in C_{ijk} {see eq 1} and with the restriction of $i + j + k \geq 2$.

Table 8. Computed Vertical Excitation Energies (T_v in eV) of Some Low-Lying Singlet and Triplet States of HSiCl from CASSCF/MRCI/AVQZ(spd,sp) Calculations[a] at the RCCSD(T)/AVQZ Geometry of the $\tilde{X}^1A'$ State

states	configuration	CASSCF	C_{max}[b]	MRCI	MRCI+D
$\tilde{X}^1A'$	$(13a')^2(3a'')^2$	0	0.928	0	0
$(1)^3A''$	$(13a')^1(4a'')^1$	1.48	0.937	1.649	1.684
$(1)^1A''$	$(13a')^1(4a'')^1$	2.88	0.911	2.863	2.823
$(1)^3A'$	$(13a')^1(14a')^1(3a'')^2$	4.52	0.930	4.651	4.656
$(2)^1A'$	$(13a')^1(14a')^1(3a'')^2$	5.83	0.881	5.720	5.614

[a] For the $\tilde{X}^1A'$, $(1)^3A'$, $(1)^1A''$, and $(1)^3A'$ states, the CASSCF calculations are average state calculations for four states. For the second $^1A'$ state, the CASSCF calculations are average state calculations for the $\tilde{X}^1A'$ and (2) $^1A'$ states. Only the s, p, and d functions were used for Si and Cl, and the s and p functions were used for H. [b] The largest computed CI coefficients in the MRCI calculations associated with the main electronic configuration (shown under configuration).

agreement is very good (bearing in mind that the intensity of the 0_0^0 vibrational component would be affected by the scattered excitation laser light). Specifically, in addition to the main $\tilde{A}^1A''(0,0,0) \rightarrow \tilde{X}^1A'(0,\upsilon_2'',0)$ progression, the simulated spectrum shows only one weak progression, which

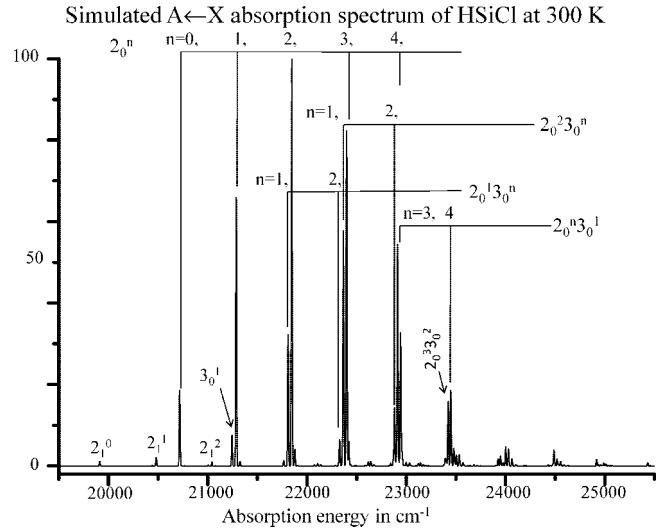

Figure 1. Simulated $\tilde{A}^1A'' \leftarrow \tilde{X}^1A'$ absorption spectrum of HSiCl at a Boltzmann vibrational temperature of 300 K with the assignments of some major vibrational progressions.

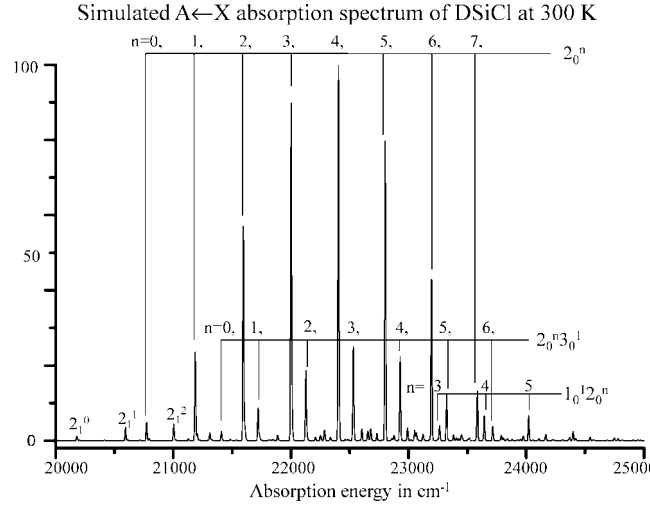

Figure 2. Simulated $\tilde{A}^1A'' \leftarrow \tilde{X}^1A'$ absorption spectrum of DSiCl at a Boltzmann vibrational temperature of 300 K with the assignments of some major vibrational progressions.

is $\tilde{A}^1A''(0,0,0) \rightarrow \tilde{X}^1A'(0,\upsilon_2'',1)$, in agreement with the experimental spectrum. Also shown in Figure 5 are the simulated spectra reported in ref 2 obtained employing the harmonic oscillator model (bottom and second from bottom traces in Figure 5; see ref 2 for details of the spectral simulations). Comparison between all the simulated and experimental spectra shows clearly that the simulated spectrum reported here, which includes anharmonicity, is superior to previously simulated spectra, which have ignored anharmonicity. Moreover, a more detailed comparison between the simulated spectrum obtained here (top trace in Figure 5) and the experimental SVL emission spectrum reported in ref 2 (second from top trace in Figure 5) suggests a gradual loss of intensity in the experimental spectrum toward low emission energy (i.e., larger displacement from the excitation line). Specifically, the strongest vibrational component in the simulated spectrum (top trace in Figure 5) is the $\tilde{A}^1A''(0,0,0) \rightarrow \tilde{X}^1A'(0,3,0)$ component, while that in the experimental spectrum (second from top trace in Figure

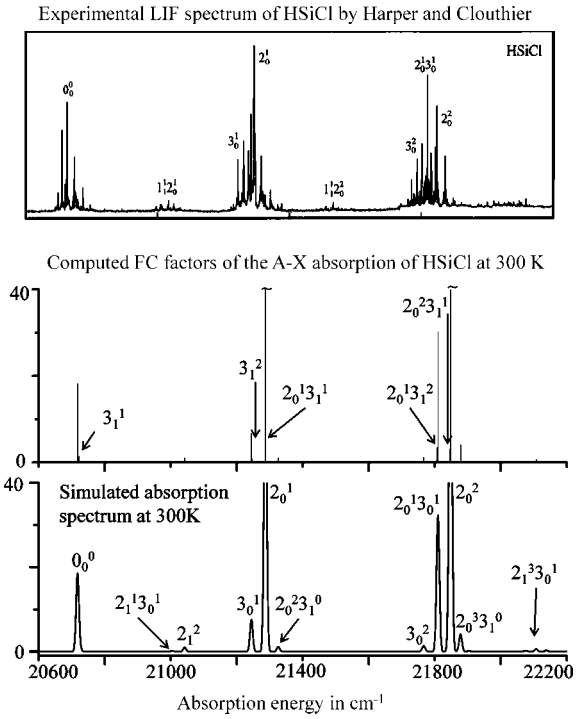

Figure 3. Computed Franck−Condon factors (the bar diagram in the middle), the simulated $\tilde{A}^1A'' \leftarrow \tilde{X}^1A'$ absorption spectrum (bottom trace) of HSiCl at a Boltzmann vibrational temperature of 300 K in the 20 600−22 200 cm^{-1} region with the assignments of some major vibrational components, and the corresponding portion of the experimental LIF spectrum of HSiCl (top trace) reported by Harper and Clouthier.[1]

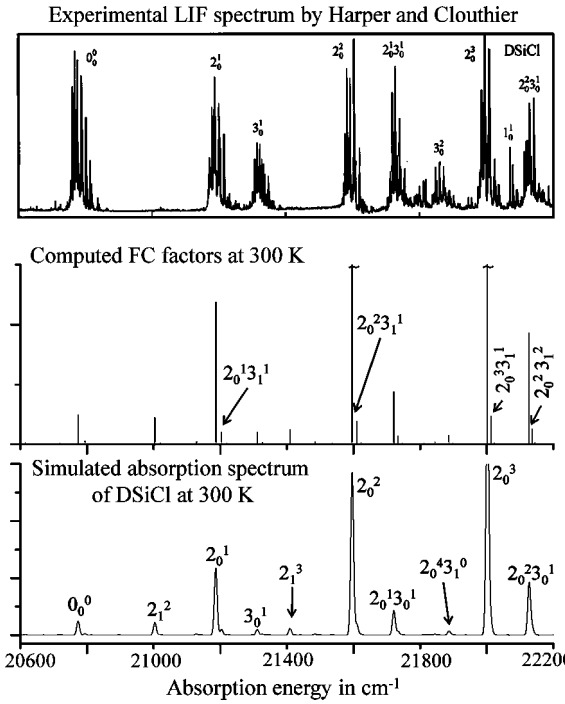

Figure 4. Computed Franck−Condon factors (the bar diagram in the middle), the simulated $\tilde{A}^1A'' \leftarrow \tilde{X}^1A'$ absorption spectrum (bottom trace) of DSiCl at a Boltzmann vibrational temperature of 300 K in the 20600−22200 cm^{-1} region with the assignments of some major vibrational components, and the corresponding portion of the experimental LIF spectrum of DSiCl (top trace) reported by Harper and Clouthier.[1]

5) is the $\tilde{A}^1A''(0,0,0) \rightarrow \tilde{X}^1A'(0,2,0)$ component. In addition, for higher members of the $\tilde{A}^1A''(0,0,0) \rightarrow \tilde{X}^1A'(0,v_2'',0)$ series, the relative intensities in the simulated spectrum are slightly stronger than those in the experimental spectrum. Assuming that the experimental SVL emission spectra recorded with the type of detector used in ref 2 (a red-sensitive photomultiplier) have not been corrected for wavelength dependence of detector sensitivity, which is expected to decrease toward low emission energy (see for example ref 27), it is anticipated that the simulated spectrum obtained here using the best *ab initio* geometries would match even better the observed spectrum if the experimental spectrum were corrected for wavelength dependent detector sensitivity. The comparison between the simulated and experimental $\tilde{A}^1A''(0,0,0) \rightarrow \tilde{X}^1A'$ SVL emission spectra of DSiCl, as shown in Figure 6, yields very similar conclusions. First, the agreement between theory and experiment is very good, and would be better if the experimental spectra were corrected for wavelength dependence of detector sensitivity. Second, the excellent agreement between simulated and experimental $\tilde{A}^1A''(0,0,0) \rightarrow \tilde{X}^1A'$ SVL emission spectra of HSiCl and DSiCl leads to the conclusions that the PEFs and the best theoretical geometrical parameters employed for the two states involved in the FC factor calculations are highly reliable.

Hostutler et al.[2] have also reported the experimental $\tilde{A}^1A''(0,1,0) \rightarrow \tilde{X}^1A'$ and $\tilde{A}^1A''(0,2,1) \rightarrow \tilde{X}^1A'$ SVL emission spectra of DSiCl, and they are compared with the corresponding simulated spectra in Figures 7 and 8, respectively.

For the $\tilde{A}^1A''(0,2,1) \rightarrow \tilde{X}^1A'$ SVL emission, there are three major vibrational progressions, namely, $\tilde{A}^1A''(0,2,1) \rightarrow \tilde{X}^1A'(0,v_2'',1)$, $\tilde{A}^1A''(0,2,1) \rightarrow \tilde{X}^1A'(0,v_2'',0)$, and $\tilde{A}^1A''(0,2,1) \rightarrow \tilde{X}^1A'(0,v_2'',2)$, in both the simulated and experimental spectra (Figure 8). The strongest progression is the $\tilde{A}^1A''(0,2,1) \rightarrow \tilde{X}^1A'(0,v_2'',1)$ progression, with the 2_03_1 and 2_13_1 components being strongest in the series in both the simulated and experimental spectra. The agreement between the simulated and observed vibrational structures for this vibrational progression may be considered as acceptable. However, the overall agreement between the simulated and experimental vibrational structure of this SVL emission cannot be considered as good. For the $\tilde{A}^1A''(0,1,0) \rightarrow \tilde{X}^1A'$ SVL emission, the agreement between the simulated and experimental spectra for the relatively weak vibrational structure in the ~4000−6000 cm^{-1} region of the $\tilde{A}^1A''(0,1,0) \rightarrow \tilde{X}^1A'$ SVL emission spectrum can be considered as reasonably good (see Figure 7). However, the dominant vibrational structure of the $\tilde{A}^1A''(0,1,0) \rightarrow \tilde{X}^1A'(0,v_2'',0)$ series, for $v_2'' = 0-5$, in the 0−3000 cm^{-1} region of the simulated spectrum (top trace of Figure 7) increases in intensity and then decreases gradually, but this behavior is not displayed in the experimental spectrum (bottom trace of Figure 7). In the experimental spectrum, the 2_2^1 component is strong as in the simulated spectrum, but the 2_1^1 and 2_3^1 components are considerably weaker than those in the simulated spectrum. In addition, the 3_1 (or $2_03_1^0$) component of the $\tilde{A}^1A''(0,1,0) \rightarrow \tilde{X}^1A'(0,v_2'',1)$ series (i.e., the 2_n3_1 series, the notation used in ref 2; bottom trace of Figure 7) is very strong in the experimental spectrum, but the whole

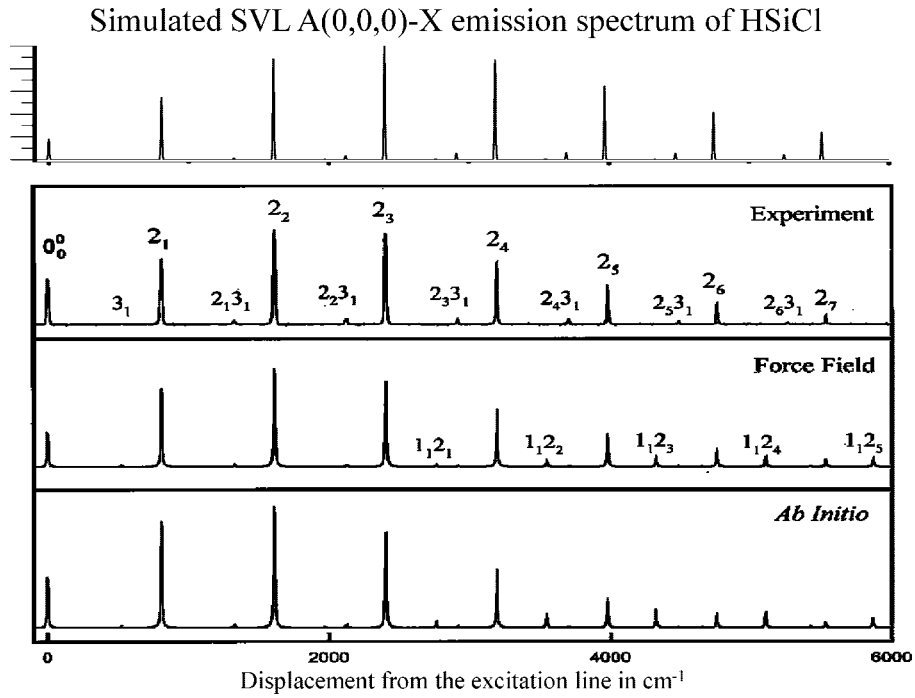

Figure 5. Simulated $\tilde{A}^1A''(0,0,0) \rightarrow \tilde{X}^1A'$ SVL emission spectrum of HSiCl (top trace) and the corresponding experimental and simulated spectra reported by Hostutler et al.[2]

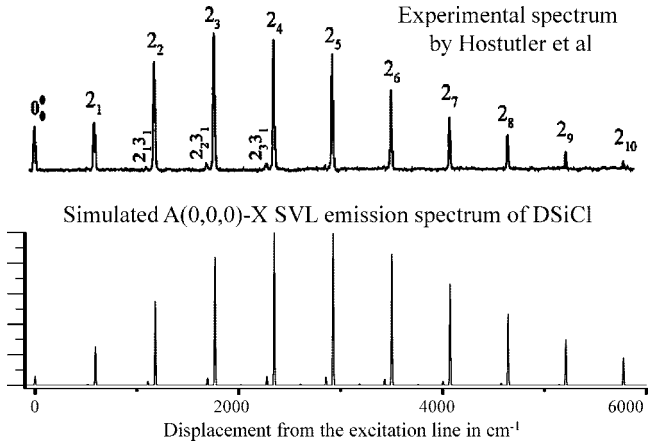

Figure 6. Simulated $\tilde{A}^1A''(0,0,0) \rightarrow \tilde{X}^1A'$ SVL emission spectrum of DSiCl (bottom trace) and the corresponding experimental and simulated spectra reported by Hostutler et al.[2] (top trace).

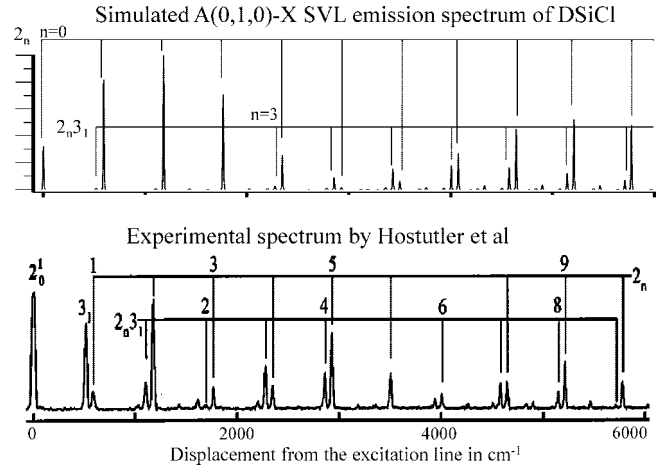

Figure 7. Simulated $\tilde{A}^1A''(0,1,0) \rightarrow \tilde{X}^1A'$ SVL emission spectrum of DSiCl and the assignments of the two major vibrational progressions (top trace) and the corresponding experimental spectrum reported by Hostutler et al.[2] (bottom trace).

$\tilde{A}^1A''(0,1,0) \rightarrow \tilde{X}^1A'(0,v_2'',1)$ series is weak in the simulated spectrum. Nevertheless, it should be noted that the energy positions of all the observed vibrational components in the two experimental SVL emission spectra of DSiCl considered, namely, the $\tilde{A}^1A''(0,1,0) \rightarrow \tilde{X}^1A'$ and $\tilde{A}^1A''(0,2,1) \rightarrow \tilde{X}^1A'$ spectra, are consistent with those of the $\tilde{X}^1A'$ state of DSiCl (see also Table 4 and discussion in Table 4 given above), suggesting that the emissions are to vibrational levels of the $\tilde{X}^1A'$ state of DSiCl, and the molecular carrier is DSiCl. The discrepancies between simulated and experimental structures of these two SVL emission spectra of DSiCl are in the relative intensities of some vibrational components. Nevertheless, in view of the fact that agreement is observed in vibrational component positions, but not in the relative intensities, it appears that, each of the two SVL emission spectra considered have major contributions from the $\tilde{A}^1A''(0,1,0) \rightarrow \tilde{X}^1A'$ and $\tilde{A}^1A''(0,2,1) \rightarrow \tilde{X}^1A'$ SVL emissions, respectively. However, the comparison between the simulated and experimental vibrational structures, as shown in Figures 7 and 8, suggests that other emissions of DSiCl are involved in the experimental spectra, that is, other states of DSiCl are accessed, as well as the $\tilde{A}^1A''(0,1,0)$ and $\tilde{A}^1A''(0,2,1)$ levels, by the excitation laser energy used to record the experimental spectra.

Concluding Remarks

In summary, high-level *ab initio* calculations have been carried out on the $\tilde{X}^1A'$ and $\tilde{A}^1A''$ states of HSiCl, and FC factors including allowance for anharmonicity have been

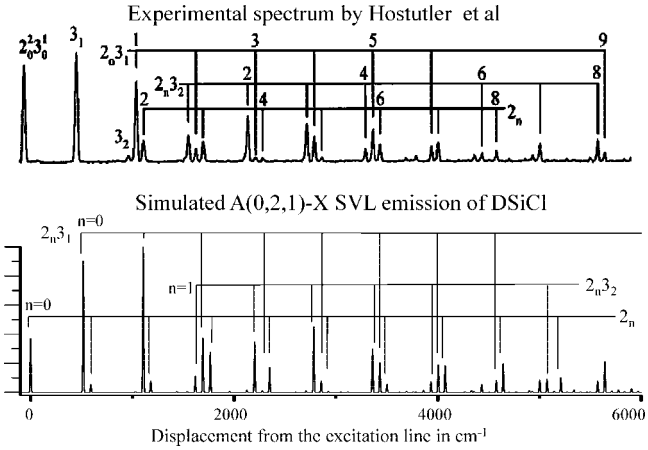

Figure 8. Simulated $\tilde{A}^1A''(0,2,1) \rightarrow \tilde{X}^1A'$ SVL emission spectrum of DSiCl and the assignments of the three major vibrational progressions (bottom trace) and the corresponding experimental spectrum reported by Hostutler et al.[2] (top trace).

computed between these two states of HSiCl and DSiCl. Agreement between theory and experiment for the minimum-energy geometrical parameters, vibrational frequencies, relative electronic energy, and the $\tilde{A}^1A''(0,0,0) \rightarrow \tilde{X}^1A'$ SVL emission spectra of HSiCl and DSiCl is very good. Simulated $\tilde{A}^1A'' \leftarrow \tilde{X}^1A'$ absorption spectra of HSiCl and DSiCl also agree reasonably well with corresponding experimental LIF spectra. Such good agreements between theory and experiment for the absorption/LIF and $\tilde{A}^1A''(0,0,0) \rightarrow \tilde{X}^1A'$ SVL emission spectra of HSiCl and DSiCl suggest that the PEFs and the best estimated geometrical parameters of the two states of HSiCl employed in the FC calculations, and the computed anharmonic vibrational wave functions and energies of the two states of HSiCl and DSiCl are highly reliable. In fact, in view of the fact that the detector employed in recording the experimental $\tilde{A}^1A''(0,0,0) \rightarrow \tilde{X}^1A'$ SVL emission spectra of HSiCl and DSiCl has a characteristic of discriminating against signals toward low emission energies and the recorded spectra have most likely not been corrected for frequency dependent sensitivity of the detector, the simulated spectra reported here are almost certainly more reliable than the experimental spectra.

However, for the $\tilde{A}^1A''(0,1,0) \rightarrow \tilde{X}^1A'$ and $\tilde{A}^1A''(0,2,1) \rightarrow \tilde{X}^1A'$ SVL emissions of DSiCl, there are significant discrepancies between simulated and experimental spectra. Specifically, the relative intensities of the simulated and experimental vibrational structures do not match very well, although the energy positions of almost all observed vibrational components agree with the computed vibrational energies of the $\tilde{X}^1A'$ state, suggesting that the emissions are to the $\tilde{X}^1A'$ state of DSiCl. It has been mentioned above in the discussion on the simulated absorption spectra of DSiCl that some hot bands are computed to be underneath some vibrational components of the main $\tilde{A}^1A'' \leftarrow \tilde{X}^1A'(0,0,0)$ absorption band. For example, for the simulated vibrational component of DSiCl at a computed absorption energy of 21186.6 cm^{-1}, in addition to the $\tilde{A}^1A''(0,1,0)'' \leftarrow \tilde{X}^1A'(0,0,0)$ transition (see Table 6 and Figure 4), the $2_0^1 3_1^1$, $1_1^1 3_0^1$, $2_2^5 3_1^0$, and $1_0^1 2_1^2 3_2^0$ hot bands with the computed absorption energies of 21203.9, 21189.4, 21183.8, and 21183.3 cm^{-1} are also expected to contribute because of the proximity of their absorption energies (though only slightly according to the computed FC factors of ~2.0, 0.002, 0.002, and 0.00005, respectively). In this connection, the dispersed fluorescence spectrum recorded at an excitation energy of 21186.6 cm^{-1} (computed value; the experimental value is 21182.08 cm^{-1}) and assigned to the $\tilde{A}^1A''(0,1,0) \rightarrow \tilde{X}^1A'$ SVL emission may have contributions also from SVL emissions from the $\tilde{A}^1A''$ (0,1,1), (1,0,1), (0,5,0), and (1,2,0) levels (being accessed via hot band transitions), in addition to the $\tilde{A}^1A''(0,1,0) \rightarrow \tilde{X}^1A'$ SVL emission. However, including these SVL emissions arising from hot band transitions in the simulation of the experimental dispersed fluorescence spectrum still did not give a satisfactory agreement between theory and experiment. Although some observed vibrational features may be accounted for by parts of the vibrational structures of these SVL emissions arising from hot bands, the overall agreement cannot be considered as good. In fact, the agreement is far from "fingerprint identification", as for the $\tilde{A}^1A''(0,0,0) \rightarrow \tilde{X}^1A'$ SVL emissions of HSiCl and DSiCl. The main difficulty, particularly in the case of the dispersed fluorescence spectrum assigned to the $\tilde{A}^1A''(0,1,0) \rightarrow \tilde{X}^1A'$ SVL emission, is that the vibrational structures of the simulated SVL emission spectra always display a gradual change in the relative intensities over a number of vibrational components (i.e., a gradual increase followed by a gradual decrease over at least four vibrational components; see for example the simulated spectra in Figures 5−8). However, the experimental $\tilde{A}^1A''(0,1,0) \rightarrow \tilde{X}^1A'$ SVL emission spectrum has the 3_1 and 2_2 vibrational components being very strong in the 2_n3_1 and 2_n series (see Figure 7 bottom trace).

To investigate this further, we have carried out preliminary calculations on some low-lying singlet and triplet states of HSiCl to see whether there are some other states nearby, which may contribute to the SVL emission spectra of HSiCl or DSiCl. Results of some CASSCF/MRCI calculations are summarized in Table 8. It can be seen that the $(1)^3A'$ and $(2)^1A'$ states are significantly higher in energy in the vertical excitation region (from the $\tilde{X}^1A'$ state) than the $\tilde{A}^1A''$ state, while the $(1)^3A''$ state is below the $\tilde{A}^1A''$ state. Further geometry optimization and vibrational frequency calculations on the lowest $^3A''$ state were carried out and gave r_e(HSi) = 1.485 Å, r(SiCl) = 2.051 Å, θ(HSiCl) = 115.5°, ω_1 = 2178 cm^{-1}, ω_2 = 652 cm^{-1}, and ω_3 = 552 cm^{-1} at the RCCSD(T)/AVQZ level. The computed T_e and T_v values at this level are 1.484 and 1.702 eV, respectively. On the basis of these calculations, it can be concluded that the lowest $^3A''$ state is the ã state, and the T_v of the $\tilde{a}^3A''$ state is ~0.84 eV (6775 cm^{-1}) below the T_0 of the $\tilde{A}^1A''$ state. Only very high vibrational levels of the $\tilde{a}^3A''$ state may overlap with low vibrational levels of the $\tilde{A}^1A''$ state, and interaction between the $\tilde{A}$ and ã vibronic levels could occur via a spin−orbit mechanism. We have also estimated the barriers to linearity of the $\tilde{X}^1A'$ (a $^1\Sigma^+$ state in $C_{\infty v}$), $\tilde{a}^3A''$ (a $^3\Pi$ state with a $\sigma^1\pi^1$ open-shell configuration) and $\tilde{A}^1A''$ states (a $^1\Pi$ state with a $\sigma^1\pi^1$ open-shell configuration) of HSiCl by carrying out CASSCF/MRCI+D/AVQZ geometry optimization calculations with the bond angle fixed to 179.5°. They are ~3.11, 2.09, and 0.74 eV above their respective potential

energy minima (the barriers to linearity of the ã and $\tilde{A}$ states are ~3.37 and 3.57 eV above the potential energy minimum of the $\tilde{X}^1A'$ state). In DSiCl, the $\tilde{A}^1A''(0,1,0)$ and $\tilde{A}^1A''(0,2,1)$ levels lie below the barriers to linearity of the $\tilde{X}$ and ã states. Interaction between vibronic levels of the ã and $\tilde{A}$ states could lead to a change in vibrational character of their vibrational levels above the minimum of the $\tilde{A}^1A''$ state and a change in FC factors in the SVL spectra from those shown in the simulated spectra in Figures 7 and 8. Clearly, further experimental and computational investigations are required to clarify the discrepancies between theory and experiment for the $\tilde{A}^1A''(0,1,0) \rightarrow \tilde{X}^1A'$ and $\tilde{A}^1A''(0,2,1) \rightarrow \tilde{X}^1A'$ SVL emission spectra of DSiCl.

Acknowledgment. Financial support from the Research Grant Council (RGC) of the Hong Kong Special Administrative Region (HKSAR, Grant PolyU 5014/06P) is acknowledged for this work. The authors are also grateful to the provision of computational resources from the EPSRC (U.K.) National Service for Computational Chemistry Software (NSCCS).

References

(1) Harper, W. W.; Clouthier, D. J. *J. Chem. Phys.* **1997**, *106*, 9461.

(2) Hostutler, D. A.; Ndiege, N.; Clouthier, D. J.; Pauls, S. W. *J. Chem. Phys.* **2001**, *115*, 5485.

(3) Lin, W.; Novick, S. E.; Fukushima, M.; Jäger, W. *J. Phys. Chem. A* **2002**, *106*, 7703.

(4) de Nalda, R.; Mavromanolakis, A.; Couris, S.; Castillejo, M. *Chem. Phys. Lett.* **2000**, *316*, 499.

(5) Vázquez, J.; Stanton, J. F. *J. Phys. Chem. A* **2002**, *106*, 4429.

(6) Coriani, S.; Marchesan, D.; Gauss, J.; Hättig, C.; Jørgensen, P.; Helgaker, T. *J. Chem. Phys.* **2005**, *123*, 184107.

(7) Rizzo, A.; Puzzarini, C.; Coriani, S.; Gauss, J. *J. Chem. Phys.* **2006**, *124*, 064302.

(8) Mok, D. K. W.; Lee, E. P. F.; Chau, F.-T.; Dyke, J. M. *J. Chem. Phys.* **2004**, *120*, 1292.

(9) (a) Hampel, C.; Peterson, K.; Werner, H.-J. *Chem. Phys. Lett.* **1992**, *190*, 1. (b) Deegan, M. J. O.; Knowles, P. J. *Chem. Phys. Lett.* **1994**, *227*, 321.

(10) Knowles, P. J.; Hampel, C.; Werner, H.-J. *J. Chem. Phys.* **1993**, *99*, 5219; Erratum. *J. Chem. Phys.* **2000**,, *112*, 3106.

(11) Werner, H.-J. *Adv. Chem. Phys.* **1987**, *LXIX*, 1.

(12) Werner, H.-J.; Knowles, P. J. *J. Chem. Phys.* **1988**, *89*, 5803.

(13) Dunning, T. H., Jr. *J. Chem. Phys.* **1989**, *90*, 1007.

(14) Dunning, T. H., Jr.; Peterson, K. A.; Wilson, A. K. *J. Chem. Phys.* **2001**, *114*, 9244.

(15) (a) Langhoff, S. R.; Davidson, E. R. *Int. J. Quantum Chem.* **1974**, *8*, 61. (b) Blomberg, M. R. A.; Siegbahn, P. E. M. *J. Chem. Phys.* **1983**, *78*, 5682. (c) Simons, J. *J. Phys. Chem.* **1989**, *93*, 626.

(16) Lee, E. P. F.; Dyke, j. M.; Chau, F.-T.; Chow, W. K. *Chem. Phys. Lett.* **2003**, *376*, 465.

(17) Halkier, A.; Helgaker, T.; Klopper, W.; Jorgensen, P.; Csaszar, A. G. *Chem. Phys. Lett.* **1999**, *310*, 385.

(18) (a) Woon, D. E.; Dunning, T. H., Jr. *J. Chem. Phys.* **1993**, *98*, 1358. (b) Peterson, K. A.; Dunning, T. H., Jr. *J. Chem. Phys.* **2002**, *117*, 10548.

(19) Werner, H.-J.; Knowles, P. J.; Lindh, R.; Manby, F. R.; Schütz, M.; Celani, P.; Korona, T.; Rauhut, G.; Amos, R. D.; Bernhardsson, A.; Berning, A.; Cooper, D. L.; Deegan, M. J. O.; Dobbyn, A. J.; Eckert, F.; Hampel, C.; Hetzer, G.; Lloyd, A. W.; McNicholas, S. J.; Meyer, W.; Mura, M. E.; Nicklass, A.; Palmieri, P.; Pitzer, R.; Schumann, U.; Stoll, H.; Stone, A. J.; Tarroni, R.; Thorsteinsson, T. *MOLPRO, A package of ab initio programs*, 2008.

(20) Carter, S.; Handy, N. C. *J. Chem. Phys.* **1987**, *87*, 4294.

(21) Dennis, J. E. Jr.; Gay, D. M.; Welsh, R. E. *ACM Trans. Math. Software* **1981**, *7*, 348–369.

(22) Watson, J. K. G. *Mol. Phys.* **1970**, *19*, 465.

(23) Mok, D. K. W.; Lee, E. P. F.; Chau, F.-T.; Wang, D.-C.; Dyke, J. M. *J. Chem. Phys.* **2000**, *113*, 5791.

(24) Chau, F.-T.; Dyke, J. M.; Lee, E. P. F.; Mok, D. K. W. *J. Chem. Phys.* **2001**, *115*, 5816.

(25) EPAPS document No. E-JCPSA6-115-001137 from http://www.aip.org/pubservs/epaps.html (accessed Nov. 20, 2008) or from ftp.aip.org in the directory /epaps/; see the EPAPS homepage of *J. Chem. Phys.* and ref 2 for more information.

(26) Experimental geometry data from NIST Computational Chemistry Comparison and Benchmark Database (http://cccbdb.nist.gov/; accessed Nov. 26, 2008);Rotational constants from Smith, J. G. *J. Mol Spectrosc.* **1986**, *120*, 110.

(27) Liu, M.-L. Lee, C.-L. Bezant, A. Tarczay, G. Clark, R. J. Miller, T. A. Chang, B.-C. PCCP, 5, 1352, 2003.

(28) Herzberg, G.; Verma, R. D. *Can. J. Phys.* **1964**, *42*, 395.

CT800513V